**Solution 3.3**

Given the definition of $S_n(e^{j\omega})$ we have

$$X_n(e^{j\omega}) = \left|S_n(e^{j\omega})\right|^2 = [S_n(e^{j\omega})][S_n(e^{j\omega})]^*$$
$$= \left[\sum_{m=-\infty}^{\infty} s(m)w(n-m)e^{-j\omega m}\right]\left[\sum_{r=-\infty}^{\infty} s(r)w(n-r)e^{j\omega r}\right]$$
$$= \sum_{r=-\infty}^{\infty}\sum_{m=-\infty}^{\infty} w(n-m)s(m)w(n-r)s(r)e^{-j\omega(m-r)}$$

Let $r = k + m$, then:

$$X_n(e^{j\omega}) = \sum_{k=-\infty}^{\infty}\left[\sum_{m=-\infty}^{\infty} s(m)w(n-m)s(m+k)\, w(n-k-m)\right]e^{j\omega k}$$
$$= \sum_{k=-\infty}^{\infty} R_n(k)e^{j\omega k} = \sum_{k=-\infty}^{\infty} R_n(k)e^{-j\omega k}$$

(since $R_n(k) = R_n(-k)$); therefore

$$X_n(e^{j\omega}) = \left|S_n(e^{j\omega})\right|^2 \overset{\text{FT}}{\longleftrightarrow} R_n(k).$$

### 3.2.2.4 FFT Implementation of Uniform Filter Bank Based on the Short-Time Fourier Transform

We now return to the question of how to efficiently implement the computation of the set of filter-bank outputs (Eq. (3.15)) for the uniform filter bank. If we assume, reasonably, that we are interested in a uniform frequency spacing—that is, if

$$f_i = i(F_s/N), \qquad i = 0, 1, \ldots, N-1 \tag{3.21}$$

then Eq. (3.15a) can be written as

$$x_i(n) = e^{j(\frac{2\pi}{N})in}\sum_m s(m)w(n-m)e^{-j(\frac{2\pi}{N})im}. \tag{3.22}$$

Now consider breaking up the summation over $m$, into a double summation of $r$ and $k$, in which

$$m = Nr + k, \quad 0 \le k \le N-1, \quad -\infty < r < \infty. \tag{3.23}$$

In other words, we break up the computation over $m$ into pieces of size $N$. If we let

$$s_n(m) = s(m)w(n-m), \tag{3.24}$$

then Eq. (3.22) can be written as

$$x_i(n) = e^{j(\frac{2\pi}{N})in}\sum_r\left[\sum_{k=0}^{N-1} s_n(Nr+k)\right]e^{-j(\frac{2\pi}{N})i(Nr+k)}. \tag{3.25}$$

Amazon / Zentian Limited
Exhibit 1013
Page 118

Since $e^{-j2\pi ir} = 1$, for all $i, r$, then

$$x_i(n) = e^{j(\frac{2\pi}{N})in} \sum_{k=0}^{N-1} \left[ \sum_r s_n(Nr + k) \right] e^{-j(\frac{2\pi}{N})ik}. \tag{3.26}$$

If we define

$$u_n(k) = \sum_r s_n(Nr + k), \qquad 0 \le k \le N - 1 \tag{3.27}$$

we wind up with

$$x_i(n) = e^{j(\frac{2\pi}{N})in} \left[ \sum_{k=0}^{N-1} u_n(k) e^{-j(\frac{2\pi}{N})ik} \right] \tag{3.28}$$

which is the desired result; that is, $x_i(n)$ is a modulated $N$-point DFT of the sequence $u_n(k)$.

Thus the basic steps in the computation of a uniform filter bank via FFT methods are as follows:

1. Form the windowed signal $s_n(m) = s(m)\, w(n - m)$, $m = n - L + 1, \ldots, n$, where $w(n)$ is a causal, finite window of duration $L$ samples. Figure 3.16a illustrates this step.
2. Form $u_n(k) = \sum_r s_n(Nr + k)$, $0 \le k \le N - 1$. That is, break the signal $s_n(m)$ into pieces of size $N$ samples and add up the pieces (alias them back unto itself) to give a signal of size $N$ samples. Figures 3.16b and c illustrate this step for the case in which $L \gg N$.
3. Take the $N$-point DFT of $u_n(k)$.
4. Modulate the DFT by the sequence $e^{j(\frac{2\pi}{N})in}$.

The modulation step 4 can be avoided by circularly shifting the sequence, $u_n(k)$, by $n \oplus N$ samples (where $\oplus$ is the modulo operation), to give $u_n((k - n))_N$, $0 \le k \le N - 1$, prior to the DFT computation.

The computation to implement the uniform filter bank via Eq. (3.28) is essentially

$$C_{\text{FBFFT}} \cong 2N \log N \cdot, +. \tag{3.29}$$

Consider now the ratio, $R$, between the computation for the direct form implementation of a uniform filter bank (Eq. (3.13)), and the FFT implementation (Eq. (3.29)), such that

$$R = \frac{C_{\text{DFFIR}}}{C_{\text{FBFFT}}} = \frac{LQ}{2N \log N}. \tag{3.30}$$

If we assume $N = 32$ (i.e., a 16-channel filter bank), with $L = 128$ (i.e., 12.8 msec impulse response filter at a 10-kHz sampling rate), and $Q = 16$ channels, we get

$$R = \frac{128 \cdot 16}{2 \cdot 32 \cdot 5} = 6.4.$$

The FFT implementation is about 6.4 times more efficient than the direct form structure.

Amazon / Zentian Limited
Exhibit 1013
Page 119

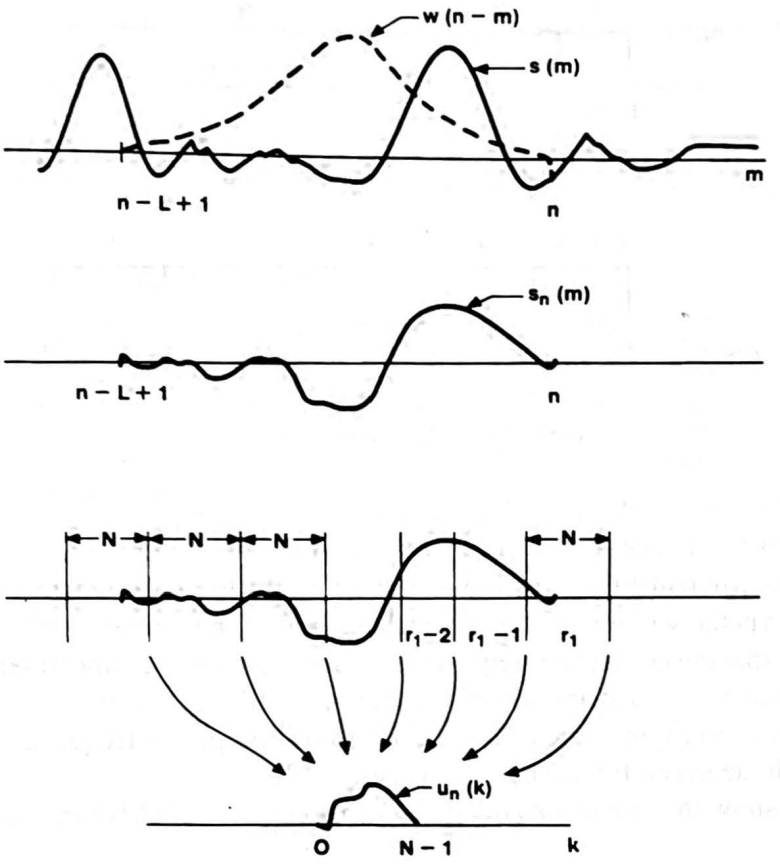



**Figure 3.16** FFT implementation of a uniform filter bank.

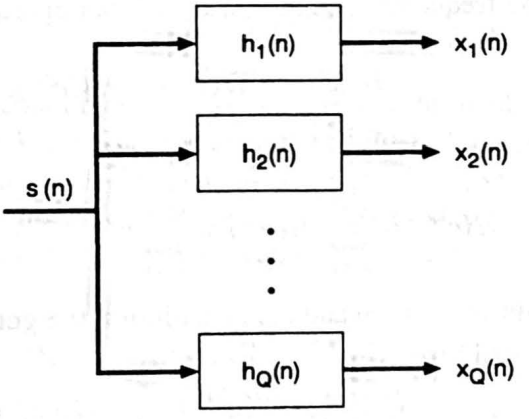



**Figure 3.17** Direct form implementation of an arbitrary nonuniform filter bank.

### 3.2.2.5 Nonuniform FIR Filter Bank Implementations

The most general form of a nonuniform FIR filter bank is shown in Figure 3.17, where the $k^{th}$ bandpass filter impulse response, $h_k(n)$, represents a filter with center frequency $\omega_k$, and bandwidth $\Delta\omega_k$. The set of $Q$ bandpass filters is intended to cover the frequency range of

Amazon / Zentian Limited
Exhibit 1013
Page 120

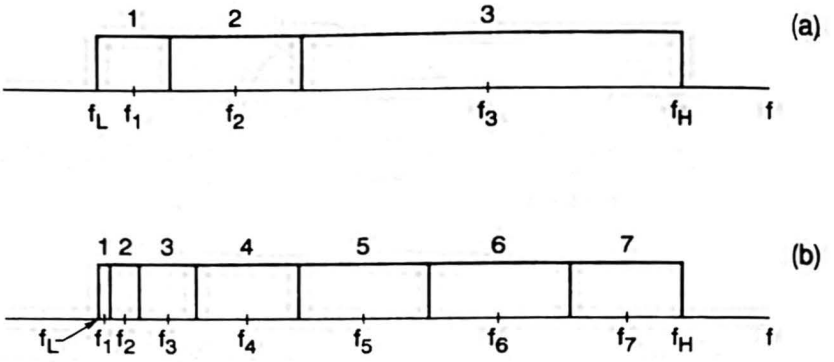



**Figure 3.18** Two arbitrary nonuniform filter-bank ideal filter specifications consisting of either 3 bands (part a) or 7 bands (part b).

interest for the intended speech-processing application.

In its most general form, each bandpass filter is implemented via a direct convolution; that is, no efficient FFT structure can be used. In the case where each bandpass filter is designed via the windowing design method (Ref. [1]), using the same lowpass window, we can show that the composite frequency response of the $Q$-channel filter bank is independent of the number and distribution of the individual filters. Thus a filter bank with the three filters shown in Figure 3.18a has the exact same composite frequency response as the filter bank with the seven filters shown in Figure 3.18b.

To show this we denote the impulse response of the $k^{\text{th}}$ bandpass filter as

$$h_k(n) = w(n)\tilde{h}_k(n), \tag{3.31}$$

where $w(n)$ is the FIR window, and $\tilde{h}_k(n)$ is the impulse response of the ideal bandpass filter being designed. The frequency response of the $k^{\text{th}}$ bandpass filter, $H_k(e^{j\omega})$, can be written as

$$H_k(e^{j\omega}) = W(e^{j\omega}) \circledast \tilde{H}_k(e^{j\omega}). \tag{3.32}$$

Thus the frequency response of the composite filter bank, $H(e^{j\omega})$, can be written as

$$H(e^{j\omega}) = \sum_{k=1}^{Q} H_k(e^{j\omega}) = \sum_{k=1}^{Q} W(e^{j\omega}) \circledast \tilde{H}_k(e^{j\omega}). \tag{3.33}$$

By interchanging the summation and the convolution we get

$$H(e^{j\omega}) = W(e^{j\omega}) \circledast \sum_{k=1}^{Q} \tilde{H}_k(e^{j\omega}). \tag{3.34}$$

By realizing that the summation of Eq. (3.34) is the summation of ideal frequency responses, we see that it is independent of the number and distribution of the individual filters. Thus we can write the summation as

$$\hat{H}(e^{j\omega}) = \sum_{k=1}^{Q} \tilde{H}_k(e^{j\omega}) = \begin{cases} 1, & \omega_{\min} \le \omega \le \omega_{\max} \\ 0, & \text{otherwise} \end{cases}, \tag{3.35}$$

Amazon / Zentian Limited
Exhibit 1013
Page 121

where $\omega_{\min}$ is the lowest frequency in the filter bank, and $\omega_{\max}$ is the highest frequency. Then Eq. (3.34) can be expressed as

$$H(e^{j\omega}) = W(e^{j\omega}) \circledast \hat{H}(e^{j\omega}) \tag{3.36}$$

independent of the number of ideal filters, $Q$, and their distribution in frequency, which is the desired result.

### 3.2.2.6 FFT-Based Nonuniform Filter Banks

One possible way to exploit the FFT structure for implementing uniform filter banks discussed earlier is to design a large uniform filter bank (e.g., $N = 128$ or 256 channels) and then create the nonuniformity by combining two or more uniform channels. This technique of combining channels is readily shown to be equivalent to applying a modified analysis window to the sequence prior to the FFT. To see this, consider taking an $N$-point DFT of the sequence $x(n)$ (derived from the speech signal, $s(n)$, by windowing by $w(n)$). Thus we get

$$X_k = \sum_{n=0}^{N-1} x(n) e^{-j\frac{2\pi}{N}nk}, \qquad 0 \le k \le N-1 \tag{3.37}$$

as the set of DFT values. If we consider adding DFT outputs $X_k$ and $X_{k+1}$, we get

$$X_k + X_{k+1} = \sum_{n=0}^{N-1} x(n) \left( e^{-j\frac{2\pi}{N}nk} + e^{-j\frac{2\pi}{N}n(k+1)} \right) \tag{3.38}$$

which can be written as

$$X'_k = X_k + X_{k+1} = \sum_{n=0}^{N-1} \left[ x(n) 2e^{-j\frac{\pi n}{N}} \cos\left(\frac{\pi n}{N}\right) \right] e^{-j\frac{2\pi}{N}nk} \tag{3.39}$$

i.e. the equivalent $k^{\text{th}}$ channel value, $X'_k$, could have been obtained by weighting the sequence, $x(n)$, in time, by the complex sequence $2e^{-j\frac{\pi n}{N}} \cos\left(\frac{\pi n}{N}\right)$. If more than two channels are combined, then a different equivalent weighting sequence results. Thus FFT channel combining is essentially a "quick and dirty" method of designing broader bandpass filters and is a simple and effective way of realizing certain types of nonuniform filter bank analysis structures.

### 3.2.2.7 Tree Structure Realizations of Nonuniform Filter Banks

A third method used to implement certain types of nonuniform filter banks is the tree structure in which the speech signal is filtered in stages, and the sampling rate is successively reduced at each stage for efficiency of implementation. An example of such a realization is given in Figure 3.19a for the 4-band, octave-spaced filter bank shown (ideally) in Figure 3.19b. The original speech signal, $s(n)$, is filtered initially into two bands, a low band and a high band, using quadrature mirror filters (QMFs)—i.e., filters whose frequency responses are complementary. The high band, which covers half the spectrum, is reduced in sampling rate by a factor of 2, and represents the highest octave band ($\pi/2 \le \omega \le \pi$) of

Amazon / Zentian Limited
Exhibit 1013
Page 122

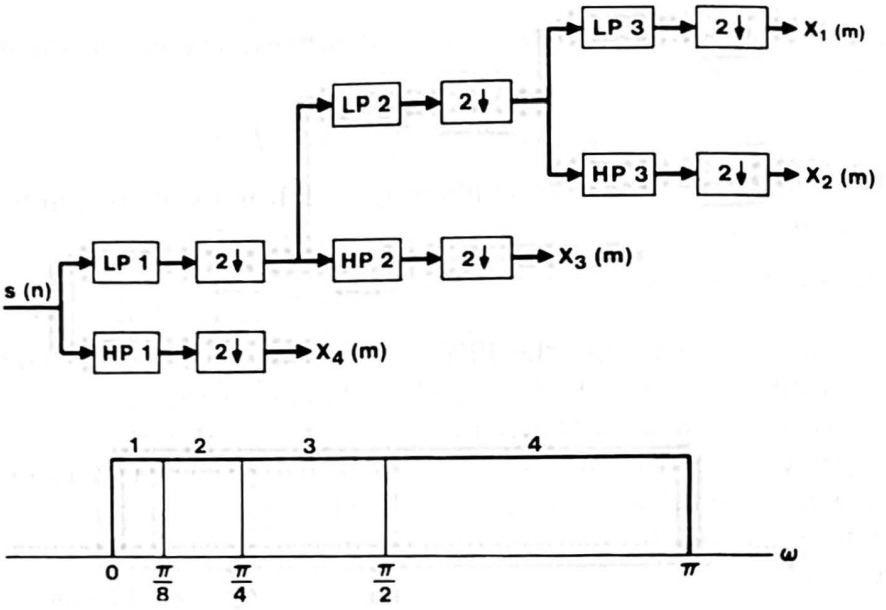



**Figure 3.19** Tree structure implementation of a 4-band, octave-spaced, filter bank.

the filter bank. The low band is similarly reduced in sampling rate by a factor of 2, and is fed into a second filtering stage in which the signal is again split into two equal bands using QMF filters. Again the high band of stage 2 is decimated by a factor of 2 and is used as the next-highest filter bank output; the low band is also decimated by a factor of 2 and fed into a third stage of QMF filters. These third-stage outputs, in this case after decimation by a factor of 2, are used as the two lowest filter bands.

QMF filter bank structures are quite efficient and have been used for a number of speech-processing applications [3]. Their efficiency for arbitrary nonuniform filter bank structures is not as good as for the octave band designs of Figure 3.19.

### 3.2.3 Summary of Considerations for Speech-Recognition Filter Banks

In the previous sections we discussed several methods of implementing filter banks for speech recognition. We have not gone into great detail here because our goal was to make the reader familiar with the issues involved in filter-bank design and implementation, not to make the reader an expert in signal processing. The interested reader is urged to pursue this fascinating area further by studying the material in the References at the end of this chapter. In this section we summarize the considerations that go into choosing the number and types of filters used in the structures discussed earlier in this section.

The first consideration for any filter bank is the type of digital filter used. The choices are IIR (recursive) and FIR (nonrecursive) designs. The IIR designs have the advantage of being implementable in simple, efficient structures. The big disadvantage of IIR filters is that their phase response is nonlinear; hence, to minimize this disadvantage

Amazon / Zentian Limited
Exhibit 1013
Page 123

a trade-off is usually made between the ideal magnitude characteristics that can readily be realized, and the highly nonideal phase characteristics. On the other hand, FIR filters can achieve linear phase without compromising the ability to approximate ideal magnitude characteristics; however, they are usually computationally expensive in implementation. For speech-recognition applications, we have shown how an FFT structure can often be applied to alleviate considerably the computational inefficiency of FIR filter banks; hence, most practical digital filter bank structures use FIR filters (usually in an FFT realization).

Once the type of filter has been decided, the next consideration is the number of filters to be used in the filter bank. For uniform filter banks, the number of filters, $Q$, cannot be too small or else the ability of the filter bank to resolve the speech spectrum is greatly impaired. Thus values of $Q$ less than about 8 are generally avoided. Similarly, the value of $Q$ cannot be too large (unless there is considerable filter overlap), because the filter bandwidths would eventually be too narrow for some talkers (e.g., high-pitch females or children), and there would be a high probability that certain bands would have extremely low speech energy (i.e., no prominent harmonic would fall within the band). Thus, practical systems tend to have values of $Q \leq 32$. Although uniformly spaced filter banks have been widely used for recognition, many practical systems have used nonuniform spacing in an effort to reduce overall computation and to characterize the speech spectrum in a manner considered more consistent with human perception.

A final consideration for practical filter-bank analyzers is the choice of nonlinearity and lowpass filter used at the output of each channel. Typically the nonlinearity has been a full wave rectifier (FWR), a half wave rectifier (HWR), or a center clipper. The resultant spectrum is only weakly sensitive to the nonlinearity. The lowpass filter used in practice varies from a simple integrator to a fairly good quality IIR lowpass filter (typically a Bessel filter).

### 3.2.4 Practical Examples of Speech-Recognition Filter Banks

Figures 3.20–3.25 [4] show examples of a wide range of speech-recognition filter banks, including both uniform and nonuniform designs. Figure 3.20 is for a 15-channel uniform filter bank in which the basic lowpass filter was designed using the windowing technique with a 101-point Kaiser window. Part a of the figure shows the impulse response of the lowpass filter (i.e., an ideal lowpass filter response multiplied by a Kaiser window). Part b of the figure shows the responses of the individual filters in the filter bank (note there is no overlap between adjacent filters), and part c shows the composite frequency response of the overall filter bank. The sidelobe peak ripple of each individual filter is down about 60 dB, and the composite frequency response is essentially ideally flat over the entire frequency range of interest (approximate 100–3000 Hz).

By contrast, Figure 3.21 is for a 15-channel uniform filter bank in which the basic lowpass filter was a Kaiser window (instead of the Kaiser windowed version of the ideal lowpass filter). From parts b and c of this figure, it can be seen that the individual bandpass filters are narrower in bandwidth than those of Figure 3.20; furthermore, the composite

Amazon / Zentian Limited
Exhibit 1013
Page 124

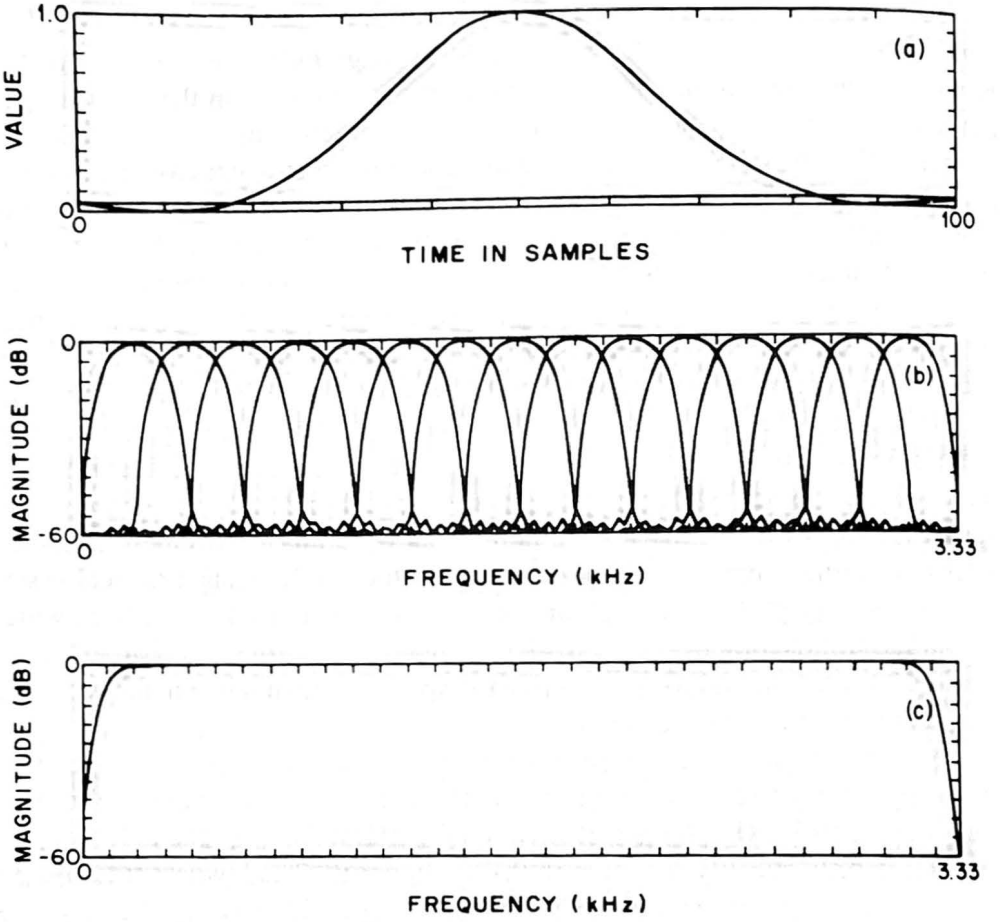



**Figure 3.20** Window sequence, $w(n)$, (part a), the individual filter response (part b), and the composite response (part c) of a $Q = 15$ channel, uniform filter bank, designed using a 101-point Kaiser window smoothed lowpass window (after Dautrich et al. [4]).

filter-bank response shows 18 dB gaps at the boundaries between each filter. Clearly, this filter bank would be unacceptable for speech-recognition applications.

Figures 3.22 and 3.23 show individual filter frequency responses, and the composite frequency response, for a 4-channel, octave-band filter bank, and a 12-channel, 1/3 octave filter bank, frequency, respectively. Each of these nonuniform filter banks was designed to cover the frequency band from 200 to 3200 Hz and used linear-phase FIR filters (101 points for the octave band design, and 201 points for the 1/3 octave band design) for each individual channel. The peak sidelobe ripple was about −40 dB for both filter banks.

Figure 3.24 shows a similar set of responses for a 7-channel critical band filter bank in which each individual filter encompassed two critical bands. Again we used 101-point, linear phase, FIR filters with a peak sidelobe of −54 dB to realize each individual bandpass filter. Finally, Figure 3.25 shows the responses of a 13-channel, critical band filter bank in which the individual channels were highly overlapping. The individual bandpass filter responses are rather poor (e.g., the ratios of center frequency to bandwidth of each filter was about 8). However, this poor frequency resolution characteristic was balanced somewhat by the excellent time resolution of the filters.

Amazon / Zentian Limited
Exhibit 1013
Page 125

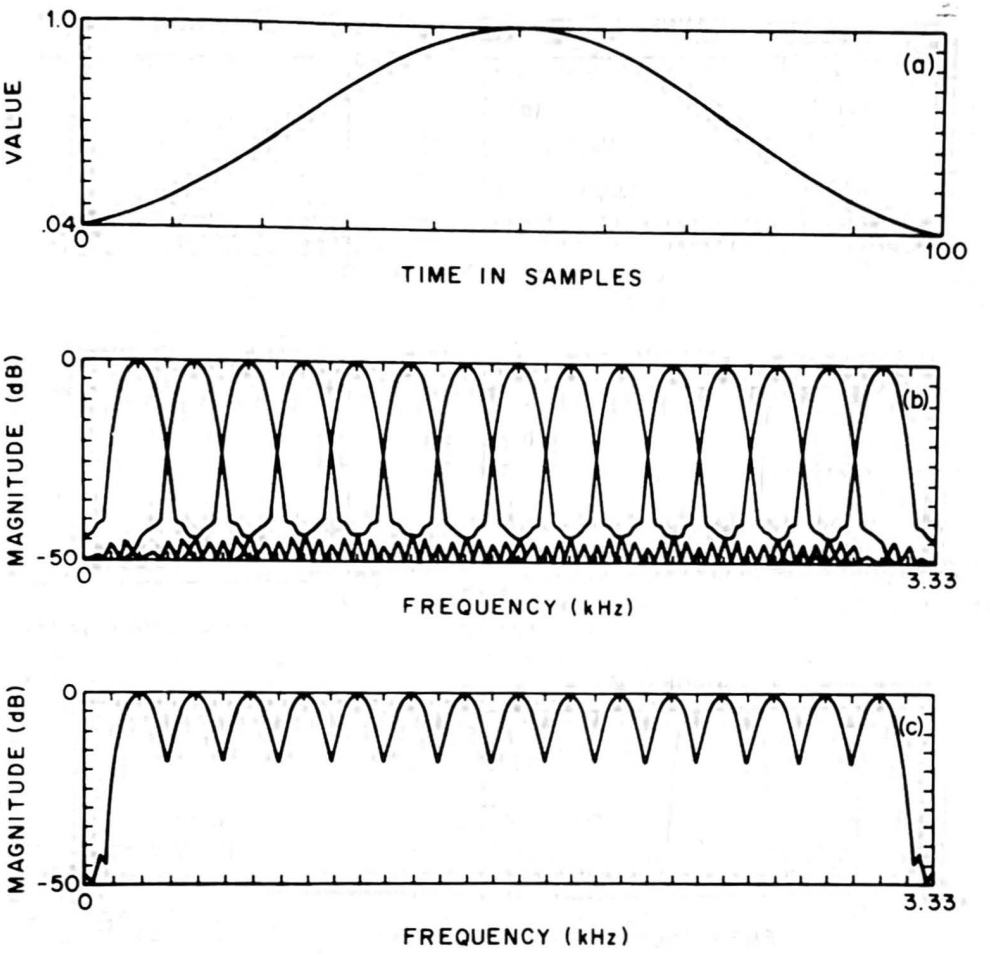



**Figure 3.21** Window sequence, $w(n)$, (part a), the individual filter responses (part b), and the composite response (part c) of a $Q = 15$ channel, uniform filter bank, designed using a 101-point Kaiser window directly as the lowpass window (after Dautrich et al. [4]).

### 3.2.5 Generalizations of Filter-Bank Analyzer

Although we have been concerned primarily with designing and implementing individual channels of a filter-bank analyzer, there is a generalized structure that must be considered as part of the canonic filter-bank analysis method. This generalized structure is shown in Figure 3.26. The generalization includes a signal preprocessor that "conditions" the speech signal, $s(n)$, to a new form, $\hat{s}(n)$, which is "more suitable" for filter-bank analysis, and a postprocessor that operates on the filter-bank output vectors, $x(m)$, to give the processed vectors $\hat{x}(m)$ that are "more suitable" for recognition. Although a wide range of signal-processing operations could go into the preprocessor and postprocessor boxes, perhaps the most reasonable ones include the following.

#### Preprocessor Operations

- signal preemphasis (to equalize the inherent spectral tilt in speech)

Amazon / Zentian Limited
Exhibit 1013
Page 126

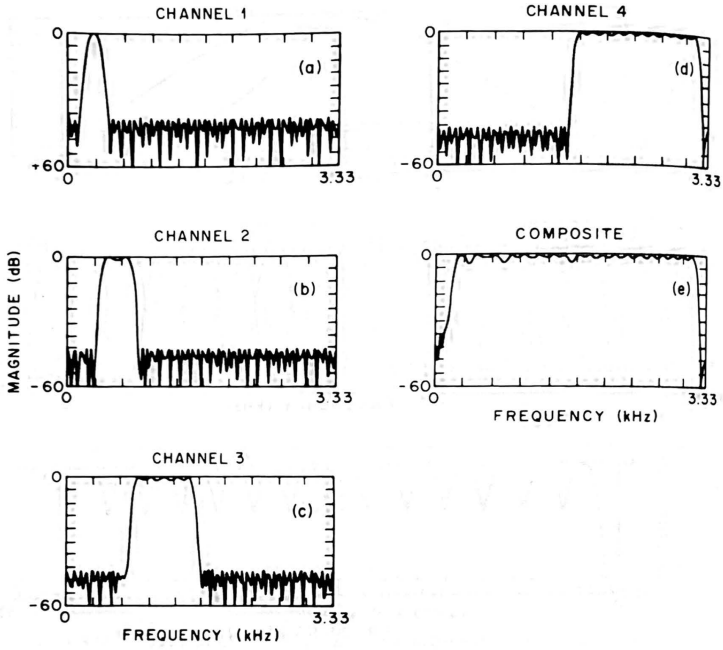



**Figure 3.22** Individual channel responses (parts a to d) and composite filter response (part c) of a $Q = 4$ channel, octave band design, using 101-point FIR filters in each band (after Dautrich et al. [4]).

- noise elimination
- signal enhancement (to make the formant peaks more prominent)

### Postprocessor Operations

- temporal smoothing of sequential filter-bank output vectors
- frequency smoothing of individual filter-bank output vectors
- normalization of each filter-bank output vector
- thresholding and/or quantization of the filter-bank output vectors
- principal components analysis of the filter-bank output vector.

The purpose of the preprocessor is to make the speech signal as clean as possible so far as the filter bank analyzer is concerned; hence, noise is eliminated, long-time spectral trends are removed, and the signal is spectrally flattened to give the best immunity to measurement imperfections. Similarly, the purpose of the postprocessor is to clean up the

Amazon / Zentian Limited
Exhibit 1013
Page 127

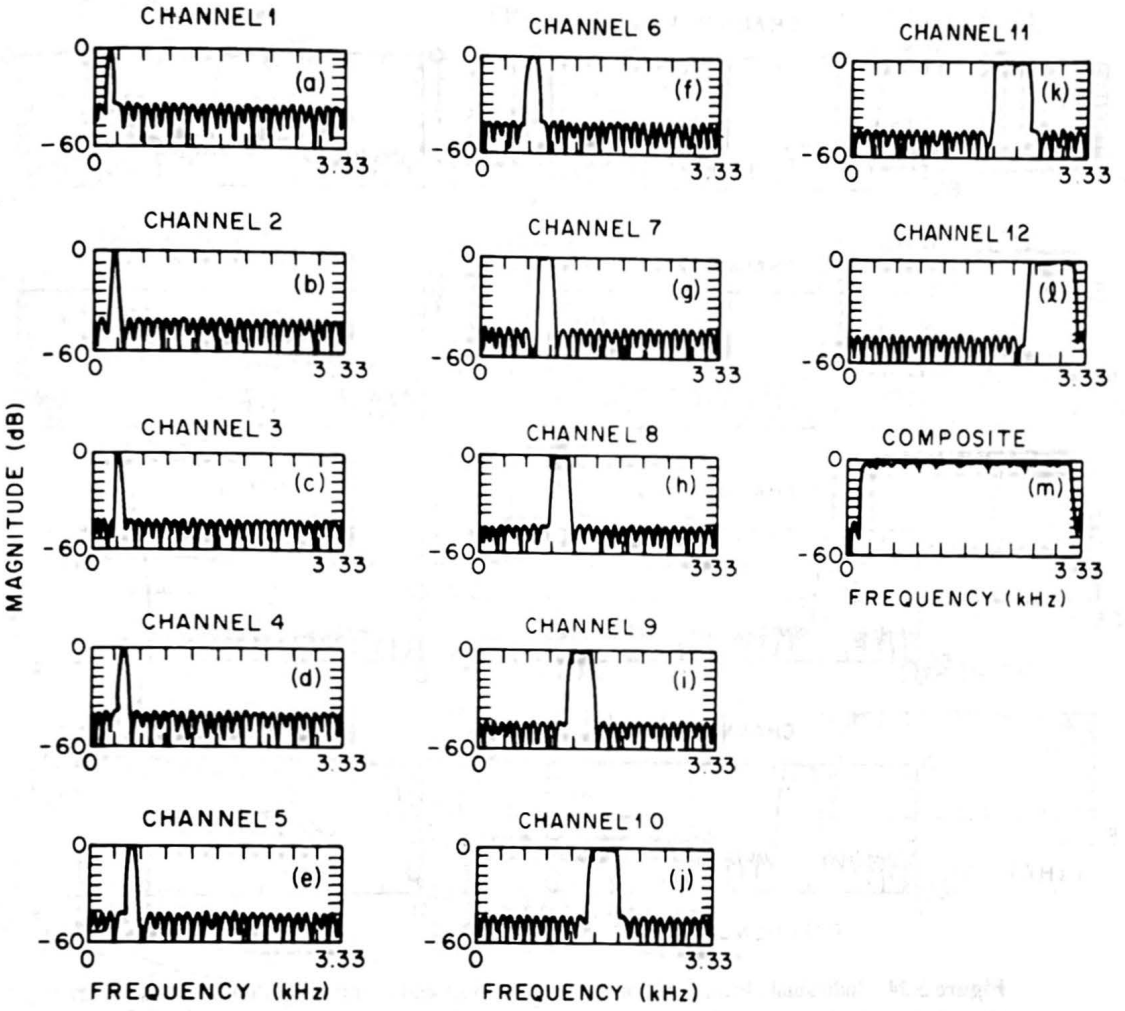



**Figure 3.23** Individual channel responses and composite filter response of a $Q = 12$ channel, 1/3 octave band design, using 201-point FIR filters in each band (after Dautrich et al. [4]).

sequence of feature vectors from the filter-bank analyzer so as to best represent the spectral information in the speech signal and thereby to maximize the chances of successful speech recognition [4,5].

## 3.3 LINEAR PREDICTIVE CODING MODEL FOR SPEECH RECOGNITION

The theory of linear predictive coding (LPC), as applied to speech, has been well understood for many years (see for example Ref. [6]). In this section we describe the basics of how LPC has been applied in speech-recognition systems. The mathematical details and derivations will be omitted here; the interested reader is referred to the references.

Before describing a general LPC front-end processor for speech recognition, it is worthwhile to review the reasons why LPC has been so widely used. These include the following:

Amazon / Zentian Limited
Exhibit 1013
Page 128

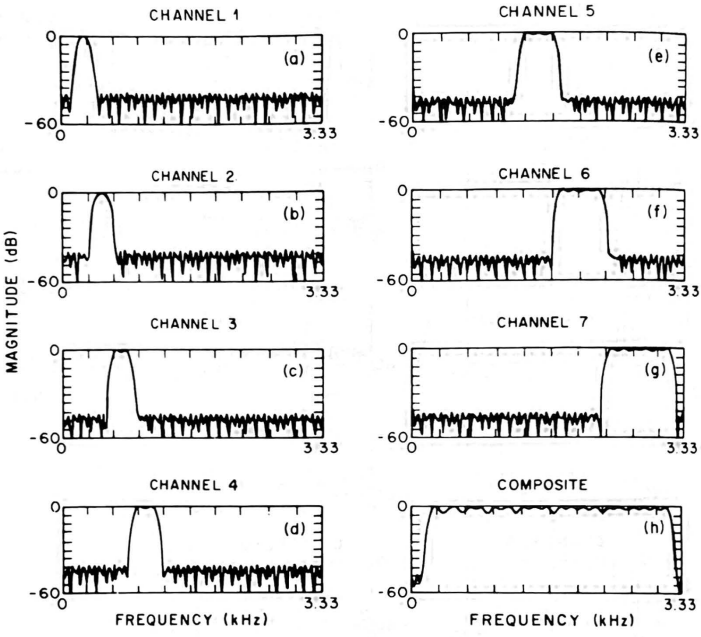



**Figure 3.24** Individual channel responses (parts a to g) and composite filter response (part h) of a $Q = 7$ channel critical band filter bank design (after Dautrich et al. [4]).

1. LPC provides a good model of the speech signal. This is especially true for the quasi steady state voiced regions of speech in which the all-pole model of LPC provides a good approximation to the vocal tract spectral envelope. During unvoiced and transient regions of speech, the LPC model is less effective than for voiced regions, but it still provides an acceptably useful model for speech-recognition purposes.
2. The way in which LPC is applied to the analysis of speech signals leads to a reasonable source-vocal tract separation. As a result, a parsimonious representation of the vocal tract characteristics (which we know are directly related to the speech sound being produced) becomes possible.
3. LPC is an analytically tractable model. The method of LPC is mathematically precise and is simple and straightforward to implement in either software or hardware. The computation involved in LPC processing is considerably less than that required for an all-digital implementation of the bank-of-filters model described in Section 3.2.
4. The LPC model works well in recognition applications. Experience has shown that

Amazon / Zentian Limited
Exhibit 1013
Page 129

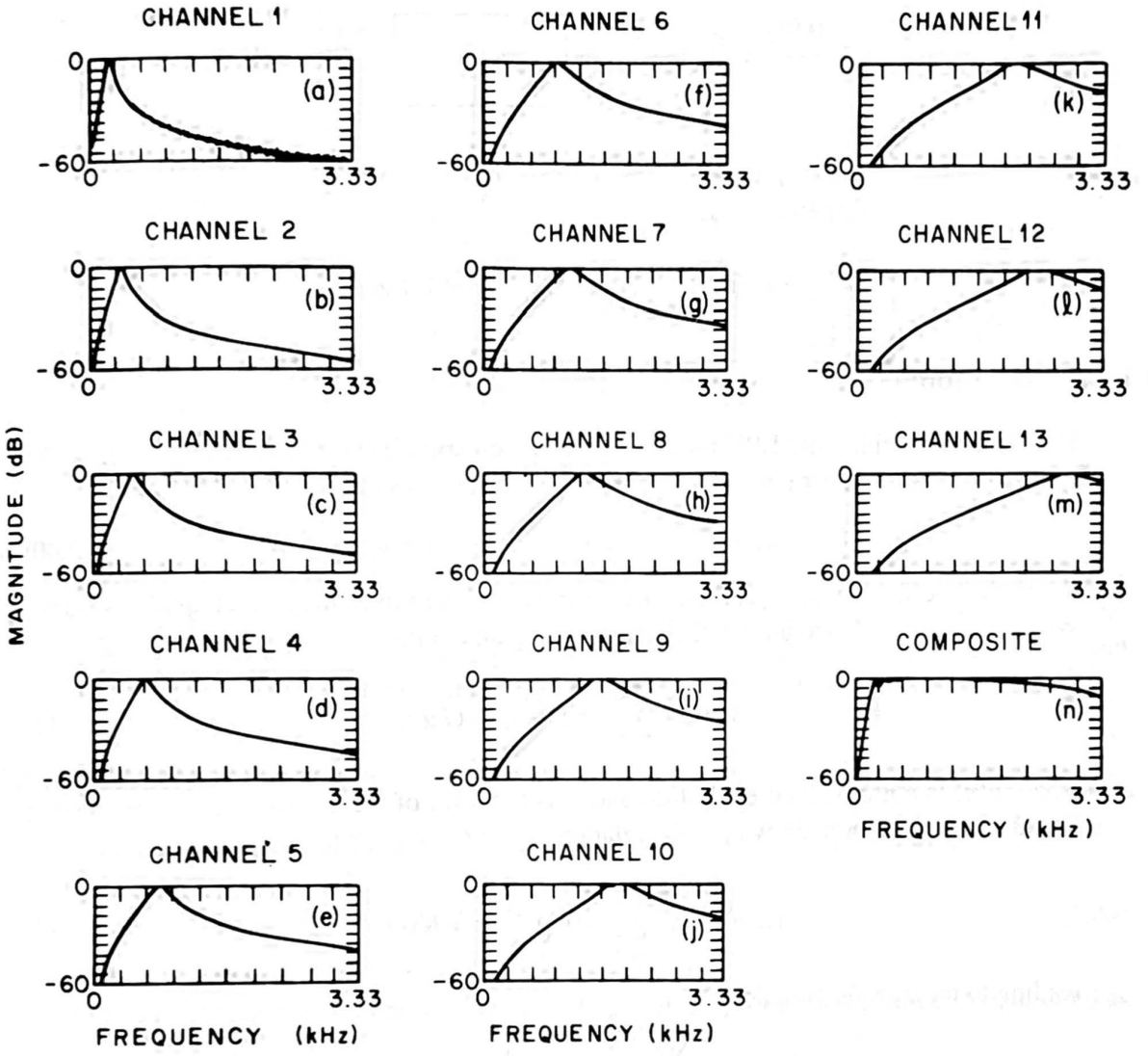



**Figure 3.25** Individual channel responses and composite filter response of a $Q = 13$ channel, critical band spacing filter bank, using highly overlapping filters in frequency (after Dautrich et al. [4]).




**Figure 3.26** Generalization of filter-bank analysis model.

the performance of speech recognizers, based on LPC front ends, is comparable to or better than that of recognizers based on filter-bank front ends (see References [4,5,7]).

Based on the above considerations, LPC front-end processing has been used in a large number of recognizers. In particular, most of the systems to be described in this book are based on this model.

Amazon / Zentian Limited
Exhibit 1013
Page 130

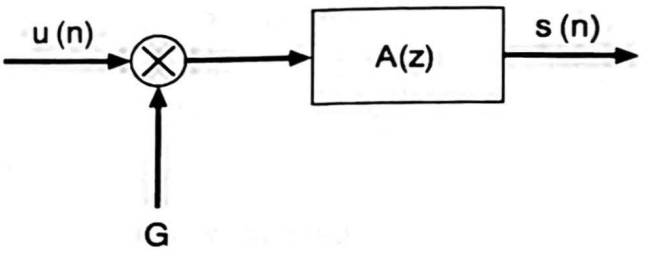



**Figure 3.27** Linear prediction model of speech.

### 3.3.1 The LPC Model

The basic idea behind the LPC model is that a given speech sample at time $n$, $s(n)$, can be approximated as a linear combination of the past $p$ speech samples, such that

$$s(n) \approx a_1 s(n-1) + a_2 s(n-2) + \cdots + a_p s(n-p), \tag{3.40}$$

where the coefficients $a_1, a_2, \ldots, a_p$ are assumed constant over the speech analysis frame. We convert Eq. (3.40) to an equality by including an excitation term, $G\,u(n)$, giving:

$$s(n) = \sum_{i=1}^{p} a_i s(n-i) + G\,u(n), \tag{3.41}$$

where $u(n)$ is a normalized excitation and $G$ is the gain of the excitation. By expressing Eq. (3.41) in the $z$-domain we get the relation

$$S(z) = \sum_{i=1}^{p} a_i z^{-i} S(z) + G\,U(z) \tag{3.42}$$

leading to the transfer function

$$H(z) = \frac{S(z)}{G\,U(z)} = \frac{1}{1 - \sum_{i=1}^{p} a_i z^{-i}} = \frac{1}{A(z)}. \tag{3.43}$$

The interpretation of Eq. (3.43) is given in Figure 3.27, which shows the normalized excitation source, $u(n)$, being scaled by the gain, $G$, and acting as input to the all-pole system, $H(z) = \frac{1}{A(z)}$, to produce the speech signal, $s(n)$. Based on our knowledge that the actual excitation function for speech is essentially either a quasiperiodic pulse train (for voiced speech sounds) or a random noise source (for unvoiced sounds), the appropriate synthesis model for speech, corresponding to the LPC analysis, is as shown in Figure 3.28. Here the normalized excitation source is chosen by a switch whose position is controlled by the voiced/unvoiced character of the speech, which chooses either a quasiperiodic train of pulses as the excitation for voiced sounds, or a random noise sequence for unvoiced sounds. The appropriate gain, $G$, of the source is estimated from the speech signal, and the scaled source is used as input to a digital filter ($H(z)$), which is controlled by the vocal tract

Amazon / Zentian Limited
Exhibit 1013
Page 131

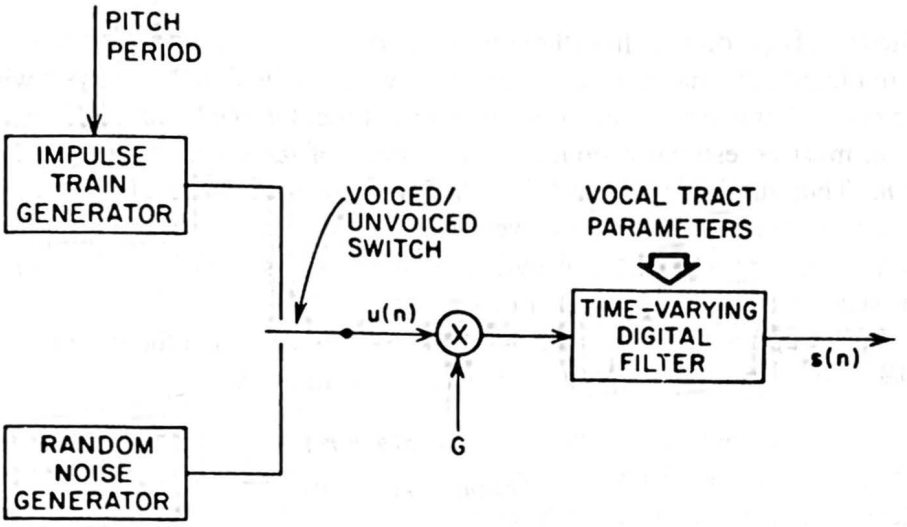



**Figure 3.28** Speech synthesis model based on LPC model.

parameters characteristic of the speech being produced. Thus the parameters of this model are voiced/unvoiced classification, pitch period for voiced sounds, the gain parameter, and the coefficients of the digital filter, $\{a_k\}$. These parameters all vary slowly with time.

### 3.3.2 LPC Analysis Equations

Based on the model of Figure 3.27, the exact relation between $s(n)$ and $u(n)$ is

$$s(n) = \sum_{k=1}^{p} a_k s(n-k) + G\,u(n). \tag{3.44}$$

We consider the linear combination of past speech samples as the estimate $\tilde{s}(n)$, defined as

$$\tilde{s}(n) = \sum_{k=1}^{p} a_k s(n-k). \tag{3.45}$$

We now form the prediction error, $e(n)$, defined as

$$e(n) = s(n) - \tilde{s}(n) = s(n) - \sum_{k=1}^{p} a_k s(n-k) \tag{3.46}$$

with error transfer function

$$A(z) = \frac{E(z)}{S(z)} = 1 - \sum_{k=1}^{p} a_k z^{-k}. \tag{3.47}$$

Clearly, when $s(n)$ is actually generated by a linear system of the type shown in Figure 3.27, then the prediction error, $e(n)$, will equal $G\,u(n)$, the scaled excitation.

The basic problem of linear prediction analysis is to determine the set of predictor

Amazon / Zentian Limited
Exhibit 1013
Page 132

coefficients, $\{a_k\}$, directly from the speech signal so that the spectral properties of the digital filter of Figure 3.28 match those of the speech waveform within the analysis window. Since the spectral characteristics of speech vary over time, the predictor coefficients at a given time, $n$, must be estimated from a *short* segment of the speech signal occurring around time $n$. Thus the basic approach is to find a set of predictor coefficients that minimize the mean-squared prediction error over a short segment of the speech waveform. (Usually this type of short time spectral analysis is performed on successive frames of speech, with frame spacing on the order of 10 msec.)

To set up the equations that must be solved to determine the predictor coefficients, we define short-term speech and error segments at time $n$ as

$$s_n(m) = s(n+m) \tag{3.48a}$$

$$e_n(m) = e(n+m) \tag{3.48b}$$

and we seek to minimize the mean squared error signal at time $n$

$$E_n = \sum_m e_n^2(m) \tag{3.49}$$

which, using the definition of $e_n(m)$ in terms of $s_n(m)$, can be written as

$$E_n = \sum_m \left[ s_n(m) - \sum_{k=1}^{p} a_k s_n(m-k) \right]^2. \tag{3.50}$$

To solve Eq. (3.50), for the predictor coefficients, we differentiate $E_n$ with respect to each $a_k$ and set the result to zero,

$$\frac{\partial E_n}{\partial a_k} = 0, \qquad k = 1, 2, \ldots, p \tag{3.51}$$

giving

$$\sum_m s_n(m-i)s_n(m) = \sum_{k=1}^{p} \hat{a}_k \sum_m s_n(m-i)s_n(m-k). \tag{3.52}$$

By recognizing that terms of the form $\sum s_n(m-i)\, s_n(m-k)$ are terms of the short-term covariance of $s_n(m)$, i.e.,

$$\phi_n(i,k) = \sum_m s_n(m-i)s_n(m-k) \tag{3.53}$$

we can express Eq. (3.52) in the compact notation

$$\boxed{\phi_n(i,0) = \sum_{k=1}^{p} \hat{a}_k \phi_n(i,k)} \tag{3.54}$$

which describes a set of $p$ equations in $p$ unknowns. It is readily shown that the minimum mean-squared error, $\hat{E}_n$, can be expressed as

Amazon / Zentian Limited
Exhibit 1013
Page 133

$$\hat{E}_n = \sum_m s_n^2(m) - \sum_{k=1}^{p} \hat{a}_k \sum_m s_n(m) s_n(m-k) \tag{3.55}$$

$$= \phi_n(0,0) - \sum_{k=1}^{p} \hat{a}_k \phi_n(0,k). \tag{3.56}$$

Thus the minimum mean-squared error consists of a fixed term ($\phi_n(0,0)$) and terms that depend on the predictor coefficients.

To solve Eq. (3.54) for the optimum predictor coefficients (the $\hat{a}_k$s) we have to compute $\phi_n(i,k)$ for $1 \leq i \leq p$ and $0 \leq k \leq p$, and then solve the resulting set of $p$ simultaneous equations. In practice, the method of solving the equations (as well as the method of computing the $\phi$s) is a strong function of the range of $m$ used in defining both the section of speech for analysis and the region over which the mean-squared error is computed. We now discuss two standard methods of defining this range for speech.

### 3.3.3 The Autocorrelation Method

A fairly simple and straightforward way of defining the limits on $m$ in the summations is to assume that the speech segment, $s_n(m)$, is identically zero outside the interval $0 \leq m \leq N-1$. This is equivalent to assuming that the speech signal, $s(m+n)$, is multiplied by a finite length window, $w(m)$, which is identically zero outside the range $0 \leq m \leq N-1$. Thus the speech sample for minimization can be expressed as

$$s_n(m) = \begin{cases} s(m+n) \cdot w(m), & 0 \leq m \leq N-1 \\ 0, & \text{otherwise.} \end{cases} \tag{3.57}$$

The effect of weighting of the speech by a window is illustrated in Figures 3.29–3.31. In each of these figures, the upper panel shows the running speech waveform, $s(m)$, the middle panel shows the weighted section of speech (using a Hamming window for $w(m)$), and the bottom panel shows the resulting error signal, $e_n(m)$, based on optimum selection of the predictor parameters.

Based on Eq. (3.57), for $m < 0$, the error signal $e_n(m)$ is exactly zero since $s_n(m) = 0$ for all $m < 0$ and therefore there is no prediction error. Furthermore, for $m > N-1+p$ there is again no prediction error because $s_n(m) = 0$ for all $m > N-1$. However, in the region of $m = 0$ (i.e., from $m = 0$ to $m = p-1$) the windowed speech signal $s_n(m)$ is being predicted from previous samples, some of which are arbitrarily zero. Hence the potential for relatively large prediction errors exists in this region and can actually be seen to exist in the bottom panel of Figure 3.29. Furthermore, in the region of $m = N-1$ (i.e., from $m = N-1$ to $m = N-1+p$) the potential of large prediction errors again exists because the zero-valued (weighted) speech signal is being predicted from at least some nonzero previous speech samples. In the bottom panel of Figure 3.30 we see this effect at the end of the prediction error waveform. These two effects are especially prominent for voiced speech when the beginning of a pitch period occurs at or very close to the $m = 0$ or $m = N-1$ points of the sample. For unvoiced speech, these problems are essentially eliminated because no part of the waveform is position sensitive. Hence we see

Amazon / Zentian Limited
Exhibit 1013
Page 134

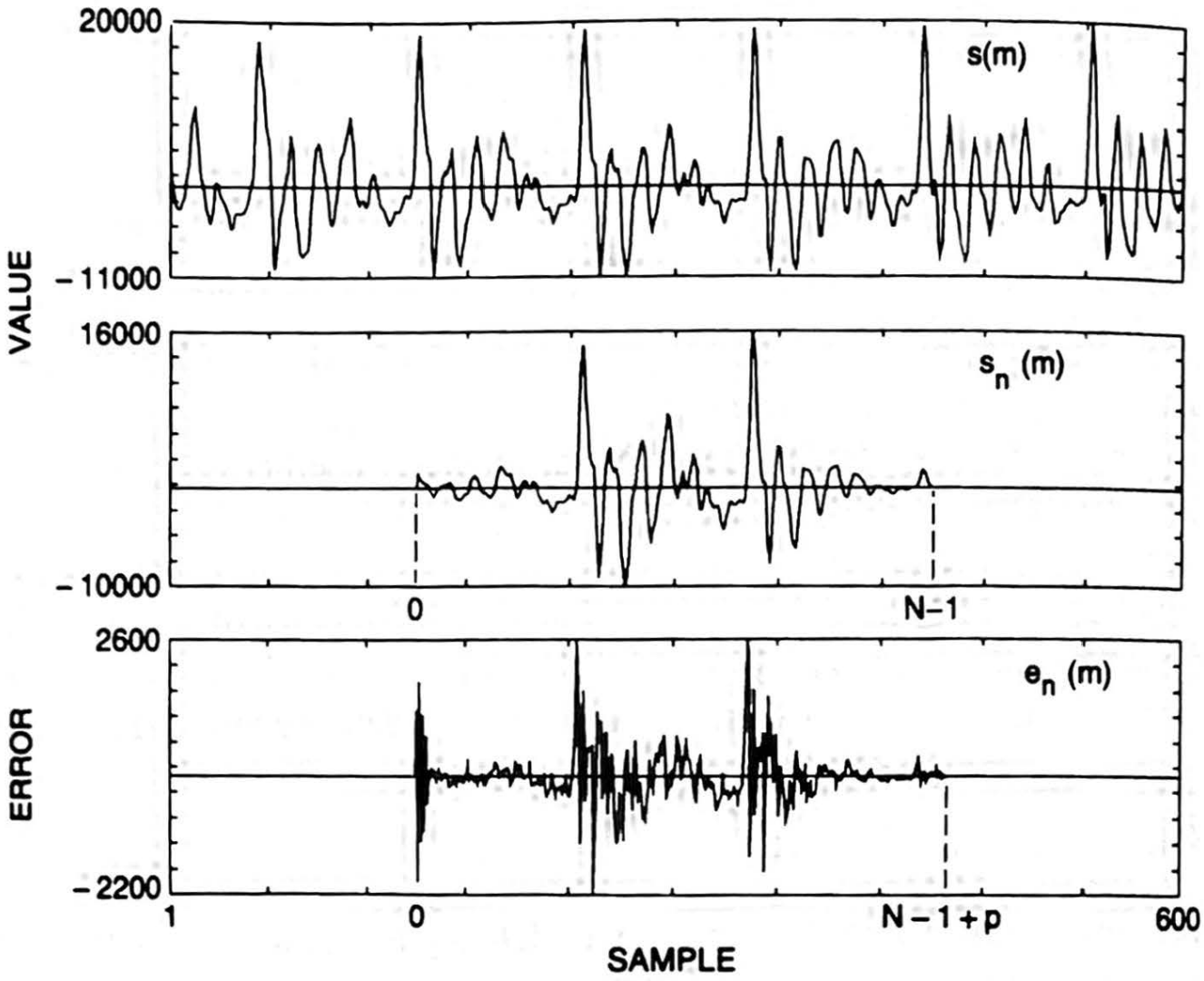



**Figure 3.29** Illustration of speech sample, weighted speech section, and prediction error for voiced speech where the prediction error is large at the beginning of the section.

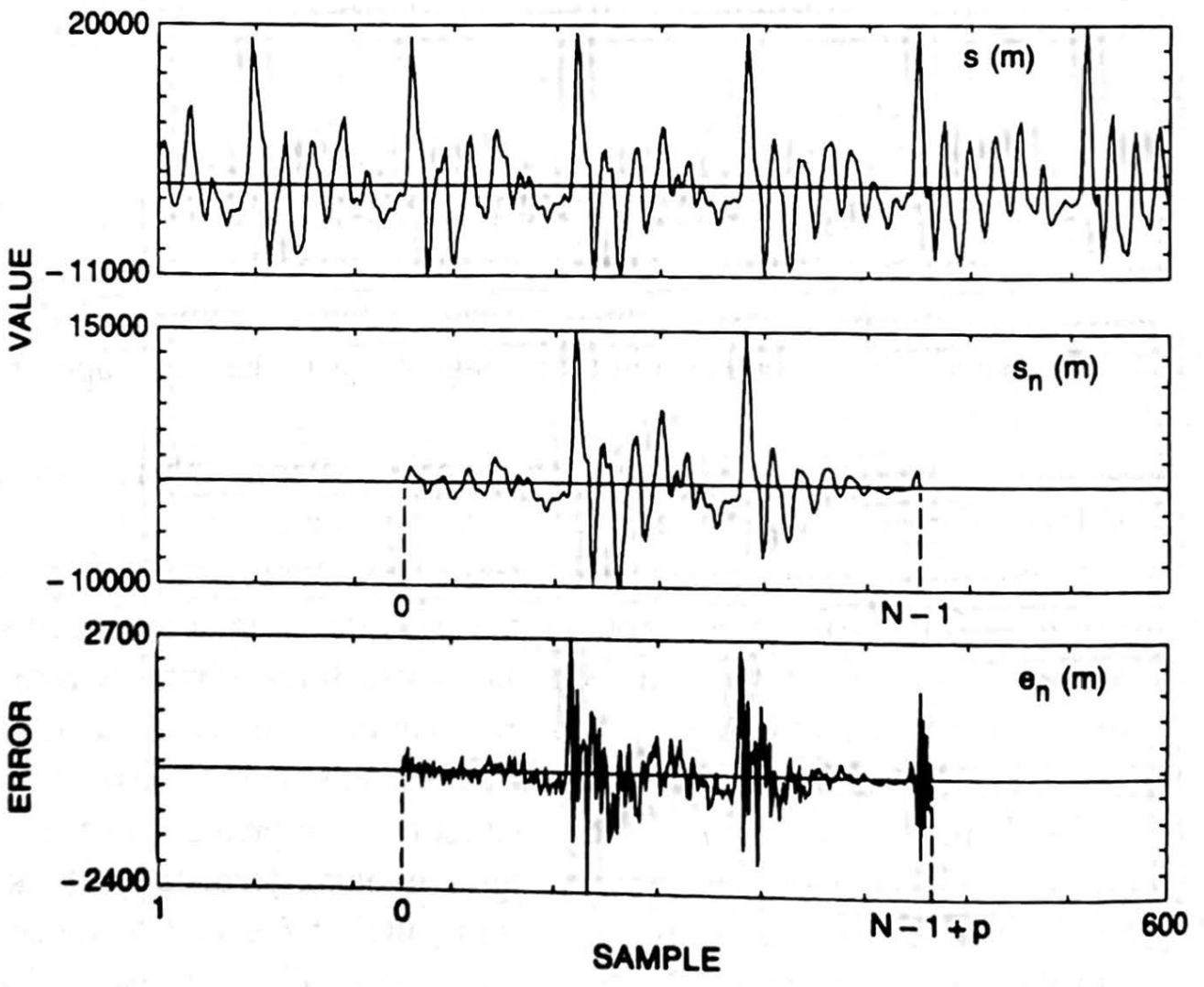



**Figure 3.30** Illustration of speech sample, weighted speech section, and prediction error for voiced speech where the prediction error is large at the end of the section.

Amazon / Zentian Limited
Exhibit 1013
Page 135

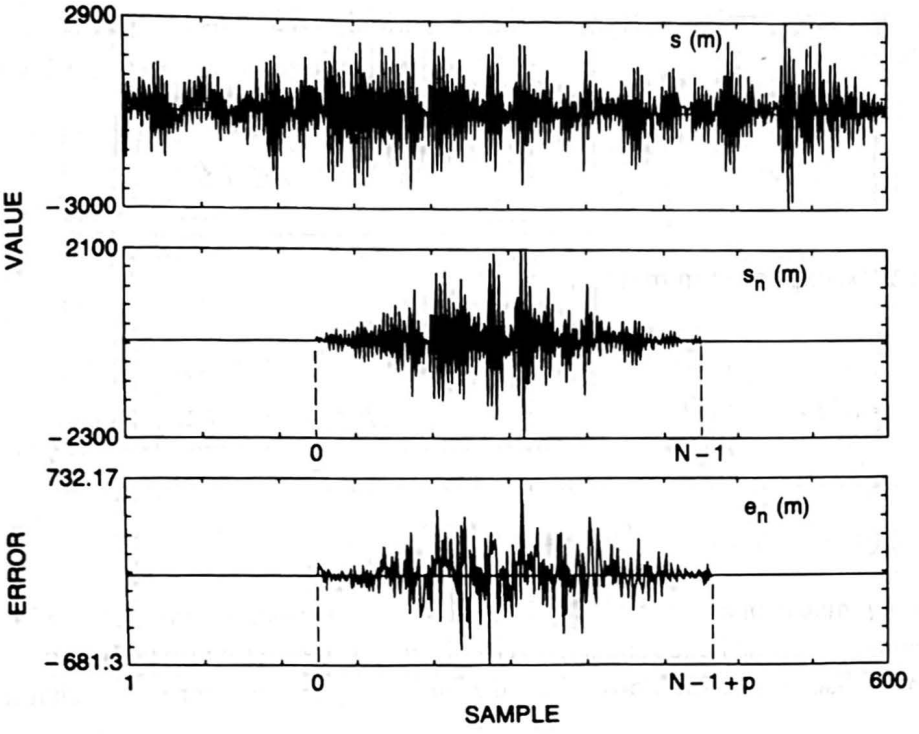



**Figure 3.31** Illustration of speech sample, weighted speech section, and prediction error for unvoiced speech where there are almost no artifacts at the boundaries of the section.

neither effect occurring in the bottom panel of Figure 3.3.1. The purpose of the window of Eq. (3.57) is to taper the signal near $m = 0$ and near $m = N - 1$ so as to minimize the errors at section boundaries.

Based on using the weighted signal of Eq. (3.57) the mean-squared error becomes

$$E_n = \sum_{m=0}^{N-1+p} e_n^2(m) \tag{3.58}$$

and $\phi_n(i,k)$ can be expressed as

$$\phi_n(i,k) = \sum_{m=0}^{N-1+p} s_n(m-i)s_n(m-k), \qquad \begin{matrix} 1 \le i \le p \\ 0 \le k \le p \end{matrix} \tag{3.59}$$

or

$$\phi_n(i,k) = \sum_{m=0}^{N-1-(i-k)} s_n(m)s_n(m+i-k), \qquad \begin{matrix} 1 \le i \le p \\ 0 \le k \le p \end{matrix} . \tag{3.60}$$

Since Eq. (3.60) is only a function of $i - k$ (rather than the two independent variables $i$ and $k$), the covariance function, $\phi_n(i,k)$, reduces to the simple autocorrelation function, i.e.,

$$\phi_n(i,k) = r_n(i-k) = \sum_{m=0}^{N-1-(i-k)} s_n(m)s_n(m+i-k). \tag{3.61}$$

Amazon / Zentian Limited
Exhibit 1013
Page 136

Since the autocorrelation function is symmetric, i.e. $r_n(-k) = r_n(k)$, the LPC equations can be expressed as

$$\boxed{\sum_{k=1}^{p} r_n(|i-k|)\hat{a}_k = r_n(i), \qquad 1 \le i \le p} \tag{3.62}$$

and can be expressed in matrix form as

$$\begin{bmatrix} r_n(0) & r_n(1) & r_n(2) & \cdots & r_n(p-1) \\ r_n(1) & r_n(0) & r_n(1) & \cdots & r_n(p-2) \\ r_n(2) & r_n(1) & r_n(0) & \cdots & r_n(p-3) \\ \vdots & \vdots & \vdots & & \vdots \\ r_n(p-1) & r_n(p-2) & r_n(p-3) & \cdots & r_n(0) \end{bmatrix} \begin{bmatrix} \hat{a}_1 \\ \hat{a}_2 \\ \hat{a}_3 \\ \vdots \\ \hat{a}_p \end{bmatrix} = \begin{bmatrix} r_n(1) \\ r_n(2) \\ r_n(3) \\ \vdots \\ r_n(p) \end{bmatrix}. \tag{3.63}$$

The $p \times p$ matrix of autocorrelation values is a Toeplitz matrix (symmetric with all diagonal elements equal) and hence can be solved efficiently through several well-known procedures. (We will discuss one such procedure, the Durbin algorithm, later in this chapter.)

### 3.3.4 The Covariance Method

An alternative to using a weighting function or window for defining $s_n(m)$ is to fix the interval over which the mean-squared error is computed to the range $0 \le m \le N-1$ and to use the unweighted speech directly—that is,

$$E_n = \sum_{m=0}^{N-1} e_n^2(m) \tag{3.64}$$

with $\phi_n(i,k)$ defined as

$$\phi_n(i,k) = \sum_{m=0}^{N-1} s_n(m-i)s_n(m-k), \qquad \begin{matrix} 1 \le i \le p \\ 0 \le k \le p \end{matrix} \tag{3.65}$$

or, by a change of variables,

$$\phi_n(i,k) = \sum_{m=-i}^{N-i-1} s_n(m)s_n(m+i-k), \qquad \begin{matrix} 1 \le i \le p \\ 0 \le k \le p \end{matrix}. \tag{3.66}$$

If we consider when $i = p$ we see that the computation of Eq. (3.66) involves speech samples $s_n(m)$ defined from $m = -p$ up to $m = N-1-p$ and, when $k = 0$, $s_n(m+i-k)$ involves samples from 0 to $N-1$. Hence the range of speech required for the complete computation is from $s_n(-p)$ to $s_n(N-1)$—that is, the samples $s_n(-p), s_n(-p+1), \ldots, s_n(-1)$, *outside* the error minimization interval, are required.

Amazon / Zentian Limited
Exhibit 1013
Page 137

Using the extended speech interval to define the covariance values, $\phi_n(i,k)$, the matrix form of the LPC analysis equations becomes

$$\begin{bmatrix} \phi_n(1,1) & \phi_n(1,2) & \phi_n(1,3) & \cdots & \phi_n(1,p) \\ \phi_n(2,1) & \phi_n(2,2) & \phi_n(2,3) & \cdots & \phi_n(2,p) \\ \phi_n(3,1) & \phi_n(3,2) & \phi_n(3,3) & \cdots & \phi_n(3,p) \\ \vdots & \vdots & \vdots & & \vdots \\ \phi_n(p,1) & \phi_n(p,2) & \phi_n(p,3) & \cdots & \phi_n(p,p) \end{bmatrix} \begin{bmatrix} \hat{a}_1 \\ \hat{a}_2 \\ \hat{a}_3 \\ \vdots \\ \hat{a}_p \end{bmatrix} = \begin{bmatrix} \phi_n(1,0) \\ \phi_n(2,0) \\ \phi_n(3,0) \\ \vdots \\ \phi_n(p,0) \end{bmatrix}. \quad (3.67)$$

The resulting covariance matrix is symmetric (since $\phi_n(i,k) = \phi_n(k,i)$) but not Toeplitz, and can be solved efficiently by a set of techniques called the Cholesky decomposition method [6]. Since the full covariance form of the LPC analysis equations is generally *not* used for speech-recognition systems, we will not discuss this method further but instead will concentrate on the autocorrelation method of LPC analysis for the remainder of this chapter.

### 3.3.5 Review Exercise

**Exercise 3.4**
Given an LPC system of the form

$$H(z) = \frac{G}{1 - \sum_{k=1}^{p} a_k z^{-k}}$$

how would you evaluate $H(e^{j\omega})$ using FFT techniques?

**Solution 3.4**
Define the LPC polynomial as

$$A(z) = \frac{G}{H(z)} = 1 - \sum_{k=1}^{p} a_k z^{-k}.$$

This finite polynomial in $z$ has a time domain response, $f(n)$, which is an FIR sequence of the form

$$f(n) = \begin{cases} 1, & n = 0 \\ -a_n, & 1 \le n \le p \\ 0, & \text{otherwise} \end{cases}.$$

Hence we can evaluate $A(e^{j\omega})$, using FFTs, by supplementing $f(n)$ with sufficient zero-valued samples to form an $N$-point sequence (e.g., $N = 256$, or $N = 512$), and taking the DFT of that sequence giving $A(e^{j\frac{2\pi}{N}k})$, $0 \le k \le N-1$, i.e. $A(e^{j\omega})|_{\omega=\frac{2\pi k}{N}}$. We can then evaluate $H(e^{j\omega})$ for $\omega = \frac{2\pi k}{N}$, $k = 0, 1, \ldots, N-1$ as $G/A(e^{j\omega})|_{\omega=\frac{2\pi k}{N}}$.

Amazon / Zentian Limited
Exhibit 1013
Page 138

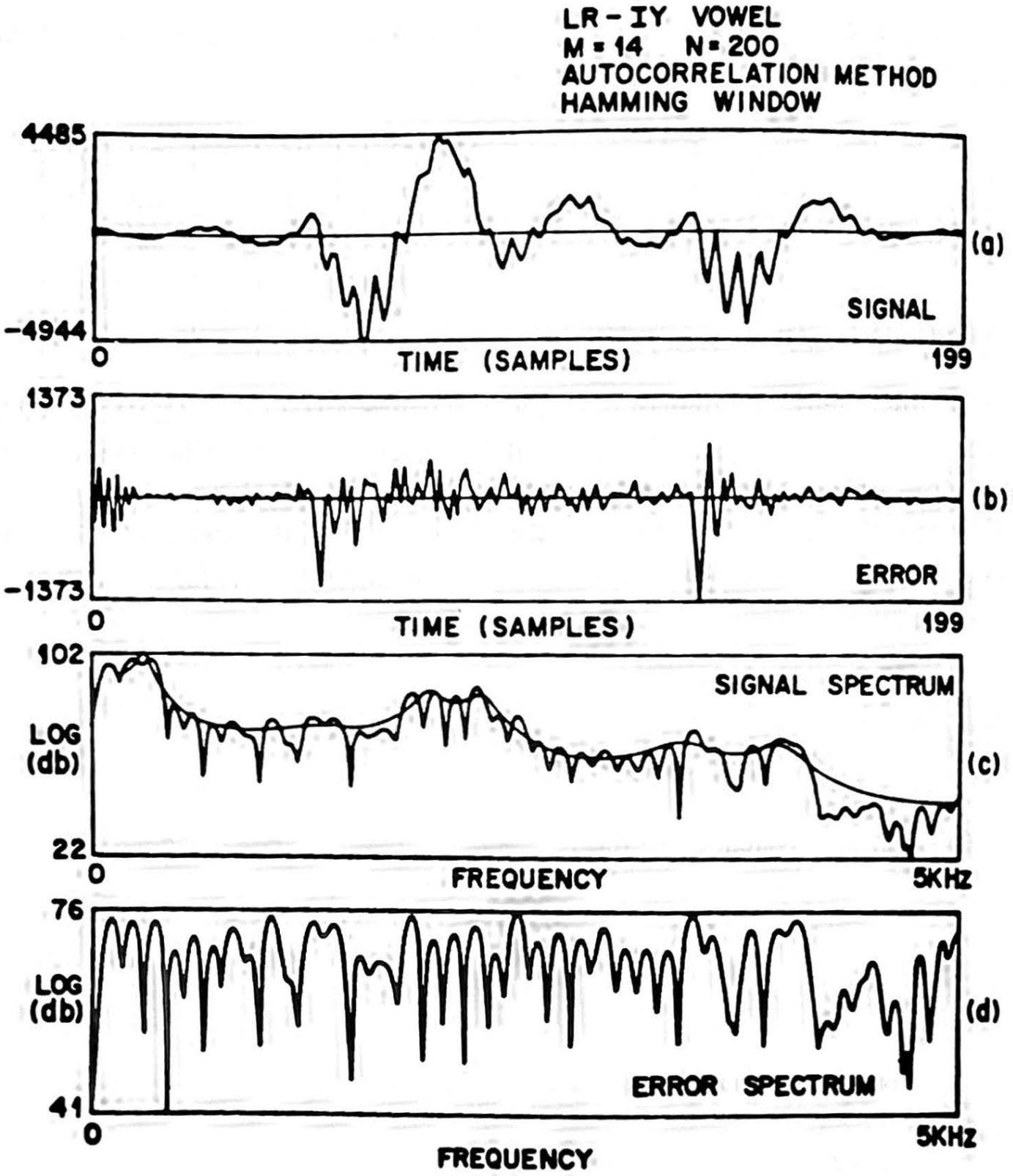



**Figure 3.32** Typical signals and spectra for LPC autocorrelation method for a segment of speech spoken by a male speaker (after Rabiner et al. [8]).

### 3.3.6 Examples of LPC Analysis

To illustrate some of the properties of the signals involved in LPC analysis, Figures 3.32 and 3.33 show series of waveform and spectral plots of the windowed speech signal (part a), the prediction error signal (part b), the signal log spectrum (FFT-based) fitted by an LPC log spectrum (as defined from Exercises 3.4, part c), and the log spectrum of the prediction error signal (part d). The results in Figure 3.32 are for the IY vowel spoken by a male speaker; those of Figure 3.33 are for the AH vowel spoken by a female speaker. For both examples the speech sample size was 20 msec (200 samples at a 10-kHz rate) and the analysis was performed using a $p = 14^{th}$ order LPC analysis. For the male speaker, about two periods of signal were used in the analysis frame. The error signal is a factor of almost 4 smaller in magnitude than the speech signal and has a much flatter spectral trend than

Amazon / Zentian Limited
Exhibit 1013
Page 139

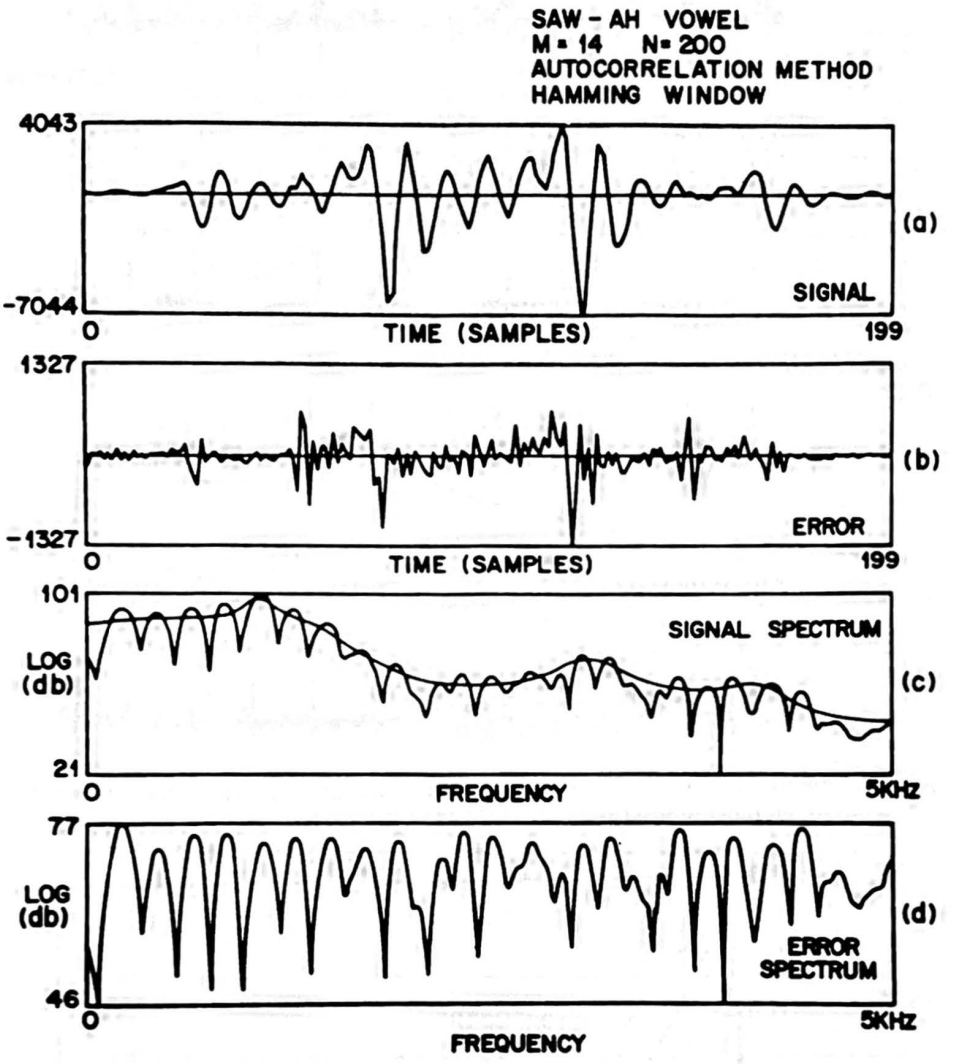



**Figure 3.33** Typical signals and spectra for LPC autocorrelation method for a segment of speech spoken by a female speaker (after Rabiner et al. [8]).

the speech signal. This is the important "whitening" characteristics of the LPC analysis whereby the error signal spectrum is approximately a flat spectrum signal representing the source characteristics rather than those of the vocal tract. Similar behavior is seen in the plots of the vowel from the female talker. Finally, it can be seen that fairly close matches exist between the peaks of the FFT-based signal spectrum and the LPC spectrum.

Figures 3.34–3.36 illustrate some additional properties of the LPC analysis method. Figure 3.34 shows a series of sections of the waveforms (differentiated for preemphasis) for several vowels, and the corresponding prediction error signals. (The prediction error signals have been scaled up in value so as to make their amplitudes comparable to those of the signal; hence, gains of about 4 to 1 were used.) The high-frequency nature of the prediction error signal is seen in all these examples. What can also be seen is that, for many cases, the prediction error signal exhibits sharp pulses at intervals corresponding to the pitch periods of these vowels. This characteristic behavior has been used as the basis

Amazon / Zentian Limited
Exhibit 1013
Page 140

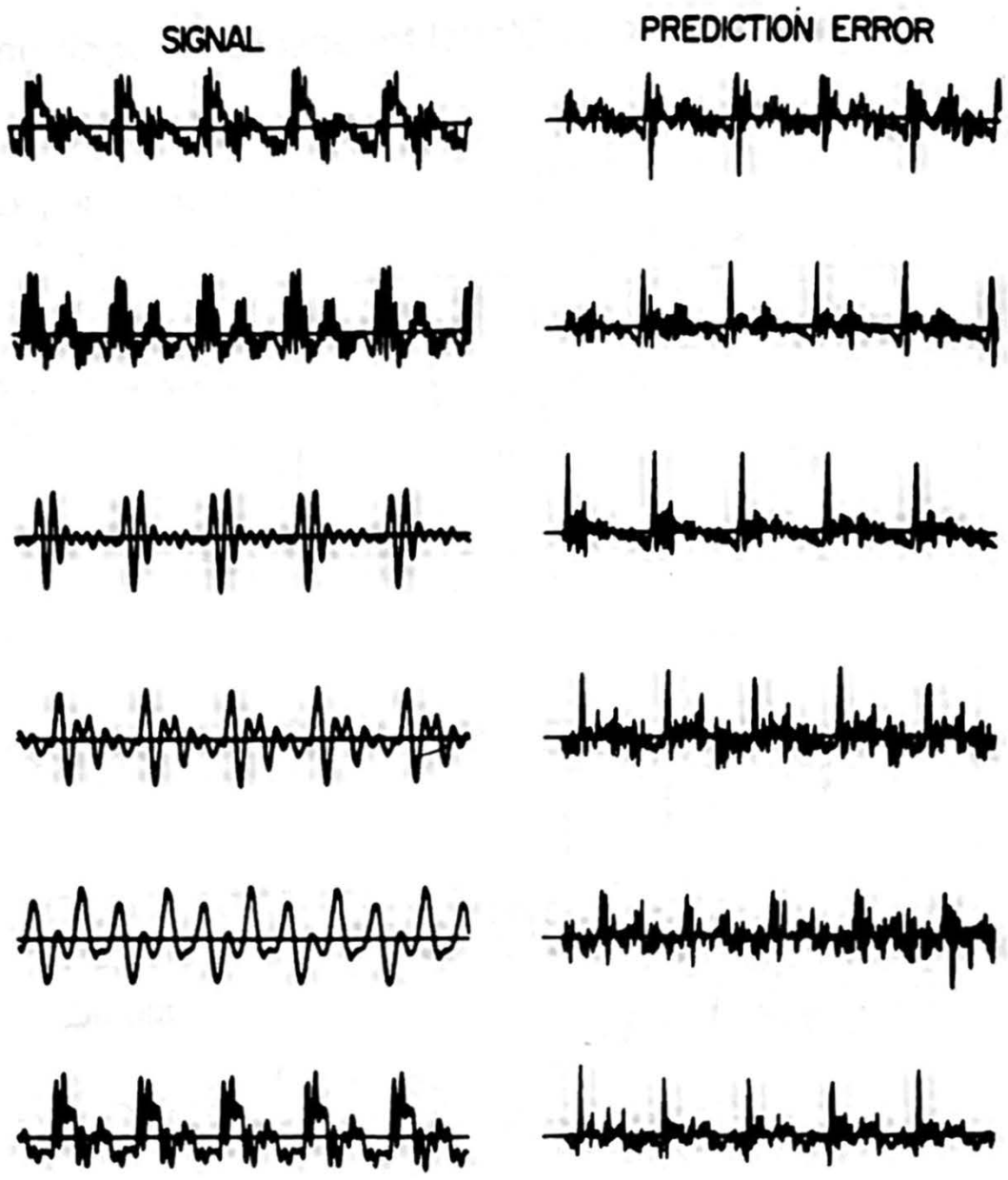



**Figure 3.34** Examples of signal (differentiated) and prediction error for several vowels (after Strube [9]).

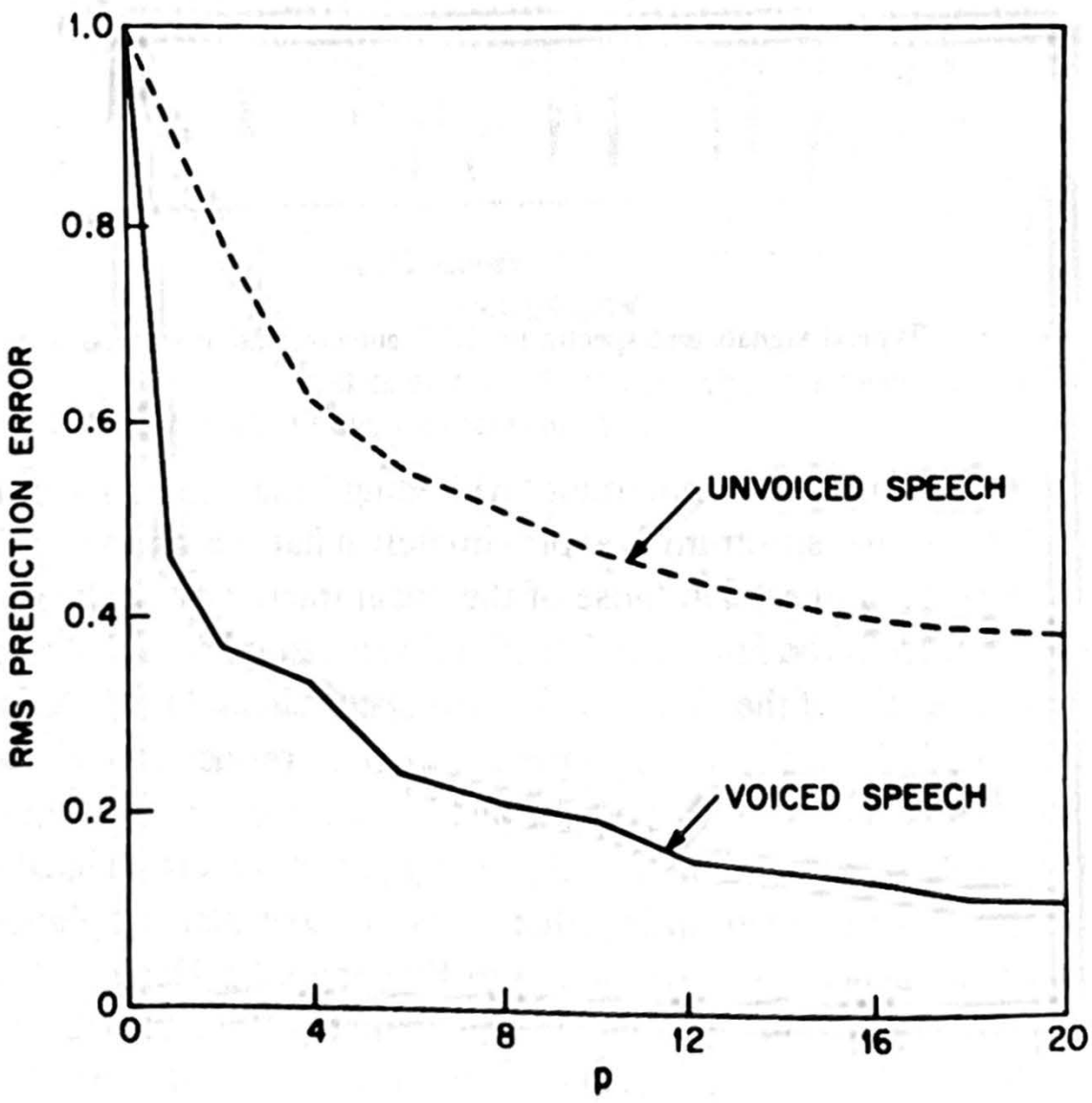



**Figure 3.35** Variation of the RMS prediction error with the number of predictor coefficients, $p$ (after Atal and Hanauer [10]).

Amazon / Zentian Limited
Exhibit 1013
Page 141

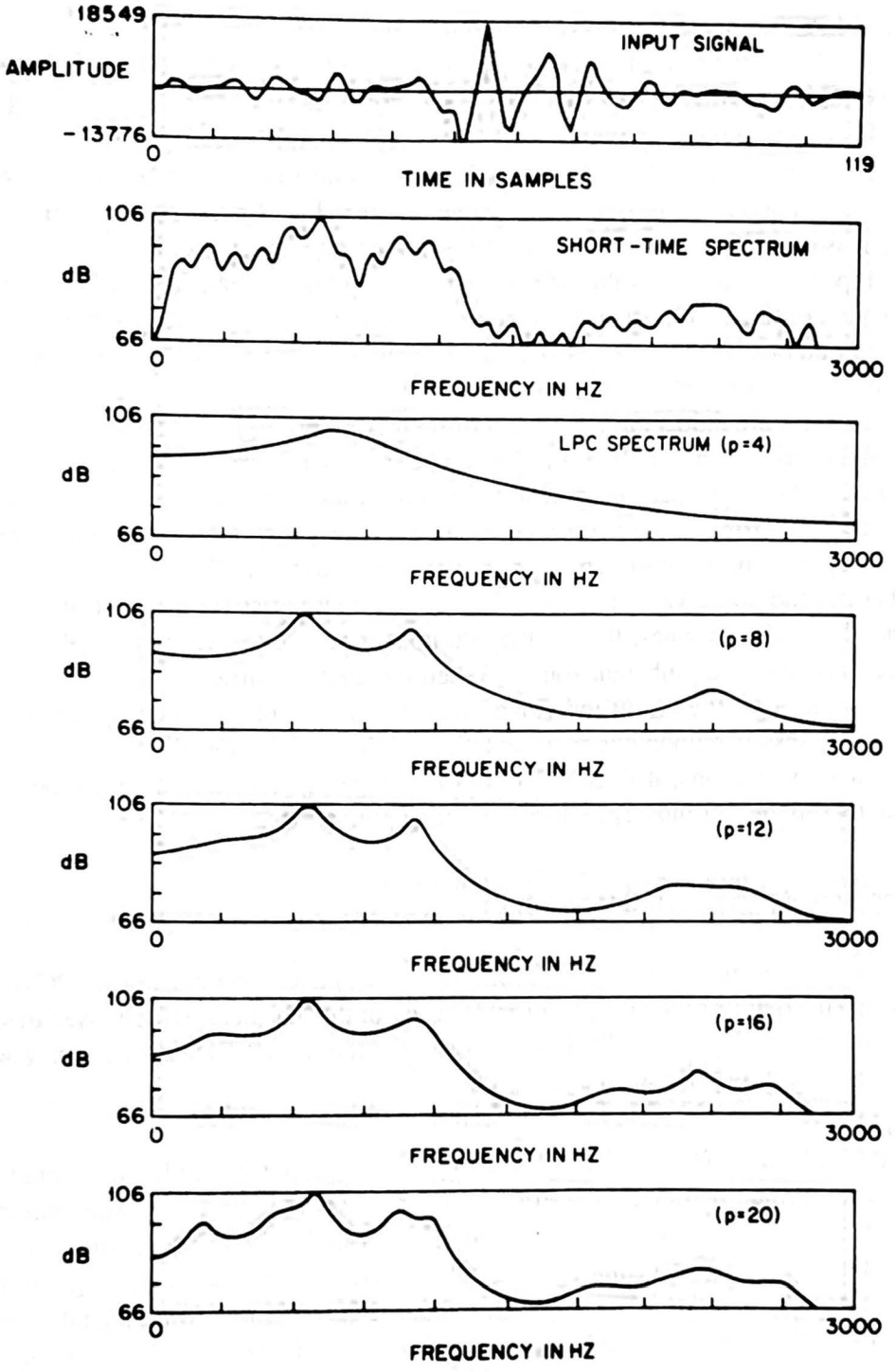



**Figure 3.36** Spectra for a vowel sound for several values of predictor order, $p$.

Amazon / Zentian Limited
Exhibit 1013
Page 142

for several LPC-based pitch period estimation methods.

Figure 3.35 shows the effect of LPC prediction order, $p$, on the RMS prediction error, $E_n$, for both sections of voiced speech (solid curve) and unvoiced speech (dashed curve). The prediction error in the curves is normalized by the signal energy such that at $p = 0$ (i.e., no prediction) $E_n = R_n(0)$. A sharp decrease in normalized prediction error occurs for small values of $p$ (e.g., 1–4); however, beyond this value of $p$ the normalized prediction error decreases much more slowly. It is also seen that the normalized prediction error for unvoiced speech, for a given value of $p$, is significantly higher than for voiced speech. The interpretation of this result is that unvoiced speech is less linearly predictable than voiced speech, a result one would anticipate based on our understanding of the speech-production mechanisms.

Finally, Figure 3.36 shows the effect of prediction order, $p$, on the all-pole spectrum and its ability to match details in the FFT spectrum of the speech segment. Shown in this figure are the input speech segment, the Fourier transform of that segment, and linear predictive spectra for values of $p$ from 4 to 20. It is clear that as $p$ increases, more of the detailed properties of the signal spectrum are preserved in the LPC spectrum. It is equally clear that beyond some value of $p$, the details of the signal spectrum that are preserved are generally irrelevant ones; that is, they do not reflect the relevant spectral resonances or antiresonances of the inherent sound. When the analysis order, $p$, becomes large, the LPC spectrum often tries to fit individual pitch harmonics of the speech signal, thereby resulting in a less parsimonious representation of the sound. On the basis of extensive experimental evaluations, it is generally acknowledged that values of $p$ on the order of 8–10 are reasonable for most speech-recognition applications.

### 3.3.7 LPC Processor for Speech Recognition

At this point, rather than spending more time discussing general properties of LPC methods, we describe the details of the LPC front-end processor that has been widely used in speech-recognition systems. Figure 3.37 shows a block diagram of the LPC processor. The basic steps in the processing include the following:

1. **Preemphasis**—The digitized speech signal, $s(n)$, is put through a low-order digital system (typically a first-order FIR filter), to spectrally flatten the signal and to make it less susceptible to finite precision effects later in the signal processing. The digital system used in the preemphasizer is either fixed or slowly adaptive (e.g., to average transmission conditions, noise backgrounds, or even to average signal spectrum). Perhaps the most widely used preemphasis network is the fixed first-order system:

$$H(z) = 1 - \tilde{a}z^{-1}, \qquad 0.9 \leq a \leq 1.0. \tag{3.68}$$

In this case, the output of the preemphasis network, $\tilde{s}(n)$, is related to the input to the network, $s(n)$, by the difference equation

$$\tilde{s}(n) = s(n) - \tilde{a}s(n-1). \tag{3.69}$$

Amazon / Zentian Limited
Exhibit 1013
Page 143

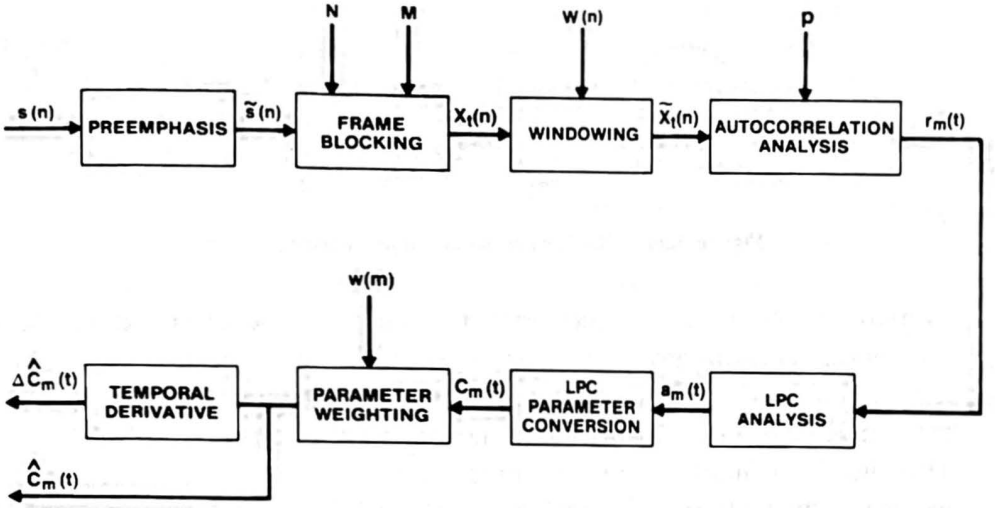



**Figure 3.37** Block diagram of LPC processor for speech recognition.

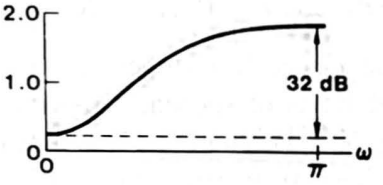



**Figure 3.38** Magnitude spectrum of LPC preemphasis network for $\tilde{a} = 0.95$.

The most common value for $\tilde{a}$ is around 0.95. (For fixed-point implementations a value of $\tilde{a} = 15/16 = 0.9375$ is often used.) A simple example of a first-order *adaptive* preemphasizer is the transfer function

$$H(z) = 1 - \tilde{a}_n z^{-1}, \tag{3.70}$$

where $\tilde{a}_n$ changes with time $(n)$ according to the chosen adaptation criterion. One possibility is to choose $\tilde{a}_n = r_n(1)/r_n(0)$. Figure 3.38 shows the magnitude characteristics of $H(e^{j\omega})$ for the value $\tilde{a} = 0.95$. It can be seen that at $\omega = \pi$ (half the sampling rate) there is a 32 dB boost in the magnitude over that at $\omega = 0$.

2. **Frame Blocking**—In this step the preemphasized speech signal, $\tilde{s}(n)$, is blocked into frames of $N$ samples, with adjacent frames being separated by $M$ samples. Figure 3.39 illustrates the blocking into frames for the case in which $M = (1/3)N$. The first illustrated frame consists of the first $N$ speech samples. The second frame begins $M$ samples after the first frame, and overlaps it by $N - M$ samples. Similarly, the third frame begins $2M$ samples after the first frame (or $M$ samples after the second frame) and overlaps it by $N - 2M$ samples. This process continues until all the speech is accounted for within one or more frames. It is easy to see that if $M \leq N$, then adjacent frames overlap (as in Figure 3.39), and the resulting LPC spectral estimates will be correlated from frame to frame; if $M \ll N$, then LPC spectral estimates from frame to frame will be quite smooth. On the other hand, if $M > N$, there will be no

Amazon / Zentian Limited
Exhibit 1013
Page 144

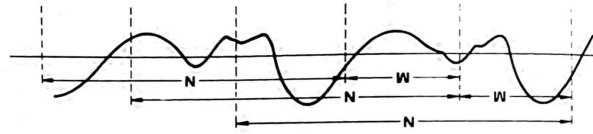



**Figure 3.39** Blocking of speech into overlapping frames.

overlap between adjacent frames; in fact, some of the speech signal will be totally lost (i.e., never appear in any analysis frame), and the correlation between the resulting LPC spectral estimates of adjacent frames will contain a noisy component whose magnitude increases as $M$ increases (i.e., as more speech is omitted from analysis). This situation is intolerable in any practical LPC analysis for speech recognition. If we denote the $\ell^{\text{th}}$ frame of speech by $x_\ell(n)$, and there are $L$ frames within the entire speech signal, then

$$x_\ell(n) = \tilde{s}(M\ell + n), \qquad n = 0, 1, \ldots, N-1, \quad \ell = 0, 1, \ldots, L-1. \tag{3.71}$$

That is, the first frame of speech, $x_0(n)$, encompasses speech samples $\tilde{s}(0), \tilde{s}(1), \ldots, \tilde{s}(N-1)$, the second frame of speech, $x_1(n)$, encompasses speech samples $\tilde{s}(M), \tilde{s}(M+1), \ldots, \tilde{s}(M+N-1)$, and the $L^{\text{th}}$ frame of speech, $x_{L-1}(n)$, encompasses speech samples $\tilde{s}(M(L-1)), \tilde{s}(M(L-1)+1), \ldots, \tilde{s}(M(L-1)+N-1)$. Typical values for $N$ and $M$ are 300 and 100 when the sampling rate of the speech is 6.67 kHz. These correspond to 45-msec frames, separated by 15 msec, or a 66.7-Hz frame rate.

3. **Windowing**—The next step in the processing is to window each individual frame so as to minimize the signal discontinuities at the beginning and end of each frame. The concept here is identical to the one discussed with regard to the frequency domain interpretation of the short-time spectrum in Section 3.2—namely, to use the window to taper the signal to zero at the beginning and end of each frame. If we define the window as $w(n)$, $0 \le n \le N-1$, then the result of windowing is the signal

$$\tilde{x}_\ell(n) = x_\ell(n) w(n), \qquad 0 \le n \le N-1. \tag{3.72}$$

A "typical" window used for the autocorrelation method of LPC (the method most widely used for recognition systems) is the Hamming window, which has the form

$$w(n) = 0.54 - 0.46 \cos\left(\frac{2\pi n}{N-1}\right), \qquad 0 \le n \le N-1. \tag{3.73}$$

4. **Autocorrelation Analysis**—Each frame of windowed signal is next autocorrelated to give

$$r_\ell(m) = \sum_{n=0}^{N-1-m} \tilde{x}_\ell(n) \tilde{x}_\ell(n+m), \qquad m = 0, 1, \ldots, p, \tag{3.74}$$

where the highest autocorrelation value, $p$, is the order of the LPC analysis. Typically, values of $p$ from 8 to 16 have been used, with $p = 8$ being the value used for most systems to be described in this book. A side benefit of the autocorrelation analysis

Amazon / Zentian Limited
Exhibit 1013
Page 145

is that the zeroth autocorrelation, $R_\ell(0)$, is the energy of the $\ell^{\text{th}}$ frame. The frame energy is an important parameter for speech-detection systems and will be discussed further in the next chapter.

5. **LPC Analysis**—The next processing step is the LPC analysis, which converts each frame of $p + 1$ autocorrelations into an "LPC parameter set," in which the set might be the LPC coefficients, the reflection (or PARCOR) coefficients, the log area ratio coefficients, the cepstral coefficients, or any desired transformation of the above sets. The formal method for converting from autocorrelation coefficients to an LPC parameter set (for the LPC autocorrelation method) is known as Durbin's method and can formally be given as the following algorithm (for convenience, we will omit the subscript $\ell$ on $r_\ell(m)$):

$$E^{(0)} = r(0) \tag{3.75}$$

$$k_i = \left\{ r(i) - \sum_{j=1}^{L-1} \alpha_j^{(i-1)} r(|i-j|) \right\} \Big/ E^{(i-1)}, \qquad 1 \le i \le p \tag{3.76}$$

$$\alpha_i^{(i)} = k_i \tag{3.77}$$

$$\alpha_j^{(i)} = \alpha_j^{(i-1)} - k_i \alpha_{i-j}^{(i-1)} \tag{3.78}$$

$$E^{(i)} = (1 - k_i^2) E^{(i-1)}, \tag{3.79}$$

where the summation in Eq. (3.76) is omitted for $i = 1$. The set of equations (3.75–3.79) are solved recursively for $i = 1, 2, \ldots, p$, and the final solution is given as

$$a_m = \text{LPC coefficients} = \alpha_m^{(p)}, \qquad 1 \le m \le p \tag{3.80}$$

$$k_m = \text{PARCOR coefficients} \tag{3.81}$$

$$g_m = \text{log area ratio coefficients} = \log \left( \frac{1 - k_m}{1 + k_m} \right). \tag{3.82}$$

6. **LPC Parameter Conversion to Cepstral Coefficients**—A very important LPC parameter set, which can be derived directly from the LPC coefficient set, is the LPC cepstral coefficients, $c(m)$. The recursion used is

$$c_0 = ln\sigma^2 \tag{3.83a}$$

$$c_m = a_m + \sum_{k=1}^{m-1} \left( \frac{k}{m} \right) c_k a_{m-k}, \qquad 1 \le m \le p \tag{3.83b}$$

$$c_m = \sum_{k=1}^{m-1} \left( \frac{k}{m} \right) c_k a_{m-k}, \qquad m > p, \tag{3.83c}$$

where $\sigma^2$ is the gain term in the LPC model. The cepstral coefficients, which are the coefficients of the Fourier transform representation of the log magnitude spectrum, have been shown to be a more robust, reliable feature set for speech recognition than the LPC coefficients, the PARCOR coefficients, or the log area ratio

Amazon / Zentian Limited
Exhibit 1013
Page 146

coefficients. Generally, a cepstral representation with $Q > p$ coefficients is used, where $Q \simeq \left(\frac{3}{2}\right) p$.

7. **Parameter Weighting**—Because of the sensitivity of the low-order cepstral coefficients to overall spectral slope and the sensitivity of the high-order cepstral coefficients to noise (and other forms of noiselike variability), it has become a standard technique to weight the cepstral coefficients by a tapered window so as to minimize these sensitivities. A formal way of justifying the use of a cepstral window is to consider the Fourier representation of the log magnitude spectrum and the differentiated (in frequency) log magnitude spectrum, such that

$$\log \left|S(e^{j\omega})\right| = \sum_{m=-\infty}^{\infty} c_m e^{-j\omega m} \tag{3.84}$$

$$\frac{\partial}{\partial \omega}\left[\log \left|S(e^{j\omega})\right|\right] = \sum_{m=-\infty}^{\infty} (-jm) c_m e^{-j\omega m}. \tag{3.85}$$

The differential log magnitude spectrum has the property that any fixed spectral slope in the log magnitude spectrum becomes a constant; furthermore, any prominent spectral peak in the log magnitude spectrum (e.g., the formants) is well preserved as a peak in the differentiated log magnitude spectrum. Hence, by considering the multiplication by $(-jm)$ in the representation of the differentiated log magnitude spectrum as a form of weighting, we get

$$\frac{\partial}{\partial \omega}\left[\log \left|S(e^{j\omega})\right|\right] = \sum_{m=-\infty}^{\infty} \hat{c}_m e^{-j\omega m}, \tag{3.86}$$

where

$$\hat{c}_m = c_m(-jm). \tag{3.87}$$

To achieve the robustness for large values of $m$ (i.e., low weight near $m = Q$) and to truncate the infinite computation of Eq. (3.86), we must consider a more general weighting of the form

$$\hat{c}_m = w_m c_m, \qquad 1 \le m \le Q, \tag{3.88}$$

where an appropriate weighting is the bandpass lifter (filter in the cepstral domain)

$$w_m = \left[1 + \frac{Q}{2} \sin\left(\frac{\pi m}{Q}\right)\right], \qquad 1 \le m \le Q. \tag{3.89}$$

This weighting function truncates the computation and de-emphasizes $c_m$ around $m = 1$ and around $m = Q$.

8. **Temporal Cepstral Derivative**—The cepstral representation of the speech spectrum provides a good representation of the local spectral properties of the signal for the given analysis frame [11]. An improved representation can be obtained by extending the analysis to include information about the temporal cepstral derivative (both first and second derivatives have been investigated and found to improve the performance of speech-recognition systems). To introduce temporal order into the

Amazon / Zentian Limited
Exhibit 1013
Page 147

cepstral representation, we denote the $m^{\text{th}}$ cepstral coefficient at time $t$ by $c_m(t)$. Of course, in practice, the sampling time $t$ refers to the analysis frame rather than an arbitrary time instance. The way in which the cepstral time derivative is approximated is as follows: The time derivative of the log magnitude spectrum has a Fourier series representation of the form

$$\frac{\partial}{\partial t}\left[\log\ |S(e^{j\omega}, t)|\right] = \sum_{m=-\infty}^{\infty} \frac{\partial c_m(t)}{\partial t} e^{-j\omega m}. \tag{3.90}$$

Hence, the temporal cepstral derivative must be determined in an appropriate manner. It is well known that since $c_m(t)$ is a discrete time representation (where $t$ is the frame index), simply using a first- or second-order difference is inappropriate to approximate the derivative (it is very noisy). Hence, a reasonable compromise is to approximate $\partial c_m(t)/\partial t$ by an orthogonal polynomial fit (a least-squares estimate of the derivative) over a finite length window; that is,

$$\frac{\partial c_m(t)}{\partial t} = \Delta c_m(t) \approx \mu \sum_{k=-K}^{K} k c_m(t+k), \tag{3.91}$$

where $\mu$ is an appropriate normalization constant and $(2K + 1)$ is the number of frames over which the computation is performed. Typically, a value of $K = 3$ has been found appropriate for computation of the first-order temporal derivative. Based on the computations described above, for each frame $t$, the result of the LPC analysis is a vector of $Q$ weighted cepstral coefficients and an appended vector of $Q$ cepstral time derivatives; that is,

$$\mathbf{o}_t' = (\hat{c}_1(t), \hat{c}_2(t), \ldots, \hat{c}_Q(t), \Delta c_1(t), \Delta c_2(t), \ldots, \Delta c_Q(t)), \tag{3.92}$$

where $\mathbf{o}_t$ is a vector with $2Q$ components and $'$ denotes matrix transpose. Similarly, if second-order temporal derivatives are computed (giving $\Delta^2 c_m(t)$), these are appended to $\mathbf{o}_t$ giving a vector with $3Q$ components (see Section 4.6 for more details).

### 3.3.8 Review Exercises

**Exercise 3.5**

To illustrate LPC analysis via the autocorrelation method, consider a predictor of order $p = 2$. Assume an autocorrelation vector with components $R = (r(0), r(1), r(2))$. Use the Durbin method, described in the previous section, to solve for the LPC coefficients $a_1$ and $a_2$ in terms of the $R$s. Check your answer by solving the matrix equation

$$\begin{bmatrix} r(0) & r(1) \\ r(1) & r(0) \end{bmatrix} \begin{bmatrix} a_1 \\ a_2 \end{bmatrix} = \begin{bmatrix} r(1) \\ r(2) \end{bmatrix}$$

using simple matrix algebra.

Amazon / Zentian Limited
Exhibit 1013
Page 148

**Solution 3.5**

Using the Durbin method, we get the following steps:

$$E^{(0)} = r(0)$$

$$k_1 = r(1)/r(0)$$
$$\alpha_1^{(1)} = r(1)/r(0)$$
$$E^{(1)} = (r^2(0) - r^2(1))/r(0)$$

$$k_2 = (r(2)r(0) - r^2(1))/(r^2(0) - r^2(1))$$
$$\alpha_2^{(2)} = (r(2)r(0) - r^2(1))/(r^2(0) - r^2(1))$$
$$\alpha_1^{(2)} = (r(1)r(0) - r(1)r(2))/(r^2(0) - r^2(1))$$

$$a_1 = \alpha_1^{(2)}$$
$$a_2 = \alpha_2^{(2)}$$

Using matrix algebra we get

$$a_1 r(0) + a_2 r(1) = r(1)$$
$$a_1 r(1) + a_2 r(0) = r(2)$$

Solving directly for $a_1$ and $a_2$ we get

$$a_1 = (r(1)r(0) - r(1)r(2))/(r^2(0) - r^2(1))$$
$$a_2 = (r(2)r(0) - r^2(1))/(r^2(0) - r^2(1))$$

which is the same result as obtained via the Durbin method.

**Exercise 3.6**

Consider two (windowed) speech sequences $x(n)$ and $\hat{x}(n)$ both defined for $0 \leq n \leq N-1$. (Outside this region both sequences are defined to be 0.) We perform an LPC analysis (using the autocorrelation method) on each frame. Thus, from the autocorrelation sequences

$$r(k) = \sum_{n=0}^{N-1-k} x(n)x(n+k), \qquad 0 \leq k \leq p$$

$$\hat{r}(k) = \sum_{n=0}^{N-1-k} \hat{x}(n)\hat{x}(n+k), \qquad 0 \leq k \leq p$$

we solve for the predictor parameter $\mathbf{a}' = (a_0, a_1, \ldots, a_p)$ and $\hat{\mathbf{a}}' = (\hat{a}_0, \hat{a}_1, \ldots, \hat{a}_p)$ ($a_0 = \hat{a}_0 = -1$) where $'$ denotes matrix transpose.

1. Show that the prediction error (residual), defined as

$$E^{(p)} = \sum_{n=0}^{N-1+p} e^2(n) = \sum_{n=0}^{N-1-p} \left[ -\sum_{i=0}^{p} a_i x(n-i) \right]^2$$

can be written in the form

$$E^{(p)} = \mathbf{a}' \mathbf{R}_x \mathbf{a},$$

Amazon / Zentian Limited
Exhibit 1013
Page 149

where $\mathbf{R}_x$ is a $(p+1)$ by $(p+1)$ matrix. Determine $\mathbf{R}_x$.

2. Consider passing the sequence $\hat{x}(n)$ through the inverse LPC system with LPC coefficients $\mathbf{a}$, to give the error signal $\tilde{e}(n)$, defined as

$$\tilde{e}(n) = -\sum_{i=0}^{p} a_i \hat{x}(n-i).$$

Show that the mean-squared error, $\tilde{E}^{(p)}$, defined by

$$\tilde{E}^{(p)} = \sum_{n=0}^{N-1+p} [\tilde{e}(n)]^2$$

can be written in the form

$$\tilde{E}^{(p)} = \mathbf{a}' \mathbf{R}_{\hat{x}} \mathbf{a},$$

where $\mathbf{R}_{\hat{x}}$ is a $(p+1)$ by $(p+1)$ matrix. Determine $\mathbf{R}_{\hat{x}}$.

3. If we form the ratio

$$D = \frac{\tilde{E}^{(p)}}{E^{(p)}}$$

what can be said about the range of $D$?

(This exercise gives an initial appreciation of the concept of distortion measures. Chapter 4 discusses this topic in great detail.)

**Solution 3.6**

1. Since

$$e(n) = -\sum_{i=0}^{p} a_i x(n-i)$$

$$E^{(p)} = \sum_{n=0}^{N-1+p} e^2(n) + \sum_{n=0}^{N-1+p} \left[-\sum_{i=0}^{p} a_i x(n-i)\right]\left[-\sum_{j=0}^{p} a_j x(n-j)\right]$$

$$= \sum_{i=0}^{p} a_i \sum_{j=0}^{p} a_j \sum_{n=0}^{N-1+p} x(n-i)x(n-j).$$

But

$$\sum_{n=0}^{N-1+p} x(n-i)x(n-j) = \sum_{n=0}^{N-1+p} x(n)x(n-j+i) = r(|i-j|).$$

Thus

$$E^{(p)} = \sum_{i=0}^{p} a_i \sum_{j=0}^{p} a_j r(|i-j|) = \mathbf{a}' \mathbf{R}_x \mathbf{a},$$

where

$$\mathbf{R}_x = \begin{bmatrix} r(0) & r(1) & \cdots & r(p) \\ r(1) & r(0) & \cdots & r(p-1) \\ \vdots & \vdots & & \vdots \\ r(p) & r(p-1) & \cdots & r(0) \end{bmatrix}$$

Amazon / Zentian Limited
Exhibit 1013
Page 150

2. $\tilde{e}(n) = -\sum_{i=0}^{p} a_i \hat{x}(n-i)$

Repeating the derivation of part 1, we get

$$\tilde{E}^{(p)} = \sum_{i=0}^{p} a_i \sum_{j=0}^{p} a_j \hat{r}(|i-j|) = \mathbf{a}' \mathbf{R}_{\hat{x}} \mathbf{a},$$

where

$$\mathbf{R}_{\hat{x}} = \begin{bmatrix} \hat{r}(0) & \hat{r}(1) & \cdots & \hat{r}(p) \\ \hat{r}(1) & \hat{r}(0) & \cdots & \hat{r}(p-1) \\ \vdots & \vdots & & \vdots \\ \hat{r}(p) & \hat{r}(p-1) & \cdots & \hat{r}(0) \end{bmatrix}$$

3. $D = \dfrac{\tilde{E}^{(p)}}{E^{(p)}} = \dfrac{\mathbf{a}' \mathbf{R}_x \mathbf{a}}{\mathbf{a}' \mathbf{R}_{\hat{x}} \mathbf{a}}$ Since $D$ is a ratio of prediction residuals, and since $E^{(p)}$ is the *minimum* prediction residual for LPC system $\mathbf{a}$, then $\tilde{E}^{(p)}$ must be greater than (or equal to) $E^{(p)}$. Therefore

$$D \geq 1.0$$

**Exercise 3.7**

A proposed measure of spectral distance between two frames of speech represented by LPC coefficient sets $\mathbf{a}$ and $\hat{\mathbf{a}}$, and augmented autocorrelation matrices $\mathbf{R}_x$ and $\mathbf{R}_{\hat{x}}$ (see Exercise 3.6) is:

$$D(\mathbf{a}, \hat{\mathbf{a}}) = \frac{\mathbf{a}' \mathbf{R}_{\hat{x}} \mathbf{a}}{\hat{\mathbf{a}}' \mathbf{R}_{\hat{x}} \hat{\mathbf{a}}}$$

1. Show that the distance function $D(\mathbf{a}, \hat{\mathbf{a}})$ can be written in the computationally efficient form

$$D(\mathbf{a}, \hat{\mathbf{a}}) = \left[ \frac{(r_a(0)\hat{r}(0) + 2\sum_{i=1}^{p} r_a(i)\hat{r}(i))}{\hat{\mathbf{a}}' \mathbf{R}_{\hat{x}} \hat{\mathbf{a}}} \right],$$

where $r_a(i)$ is the autocorrelation of the $\mathbf{a}$ array, i.e.,

$$r_a(i) = \sum_{j=0}^{p-i} a_j a_{j+i}, \qquad 0 \leq i \leq p.$$

2. Assume that the quantities (i.e., vectors, matrices, scalars) $\mathbf{a}, \hat{\mathbf{a}}, \mathbf{R}_x, \mathbf{R}_{\hat{x}}, \hat{\mathbf{a}}' \mathbf{R}_{\hat{x}} \hat{\mathbf{a}}, \mathbf{R}_{\hat{x}}$ and $\mathbf{R}_a$ are precomputed; that is, they are available at the time the distance calculation is required. Contrast the computation required to evaluate $D(\mathbf{a}, \hat{\mathbf{a}})$ using both expressions for $D$ given in this exercise.

**Solution 3.7**

We have that

$$D(\mathbf{a}, \hat{\mathbf{a}}) = \frac{\mathbf{a}' \mathbf{R}_{\hat{x}}, \mathbf{a}}{\hat{\mathbf{a}}' \mathbf{R}_{\hat{x}} \hat{\mathbf{a}}} = \frac{\tilde{E}^{(p)}}{\hat{E}^{(p)}}.$$

Amazon / Zentian Limited
Exhibit 1013
Page 151

From Exercise 3.6 we get

$$\tilde{E}^{(p)} = \sum_{i=0}^{p} a_i \sum_{j=0}^{p} a_j \hat{r}(|j-i|).$$

Letting $k = j - i$ ($j = k + i$) we get

$$\tilde{E}^{(p)} = \sum_{i=0}^{p} a_i \sum_{k=-i}^{p-i} a_{k+i} \hat{r}(|k|).$$

By rearranging the summations on $i$ and $k$ and by recognizing that $a_\ell = 0$, $\ell < 0$ and $a_\ell = 0$, $\ell > p$, we can complete the square by summing on $k$ from $-p$ (the smallest value of $k$) to $+p$ (the largest value of $k$), giving

$$\tilde{E}^{(p)} = \sum_{k=-p}^{p} \left[ \sum_{i=0}^{p-|k|} a_i a_{k+i} \right] \hat{r}(|k|).$$

The inner summation is defined as $r_a(k)$, hence

$$\tilde{E}^{(p)} = \sum_{k=-p}^{p} r_a(k) \hat{r}(|k|).$$

Since $r_a(k) = r_a(-k)$ and $\hat{r}(k) = \hat{r}(-k)$ we can write $\tilde{E}^{(p)}$ as

$$\tilde{E}^{(p)} = r_a(0)\hat{r}(0) + 2 \sum_{k=1}^{p} r_a(k)\hat{r}(k).$$

**2** Since all the individual quantities are precomputed, to evaluate $D$ as a ratio of residuals; that is,

$$D = \frac{\mathbf{a}' \mathbf{R}_{\hat{x}} \mathbf{a}}{\hat{\mathbf{a}}' \mathbf{R}_{\hat{x}} \hat{\mathbf{a}}}$$

requires

**a.** $(p + 1) \times (p + 2)$ multiplies and adds to multiply $\mathbf{a}'$ by $\mathbf{R}_{\hat{x}}$ and then multiply the result by $\mathbf{a}$.

**b.** 1 divide to give $D$ since $\hat{\mathbf{a}}' \mathbf{R}_{\hat{x}} \hat{\mathbf{a}}$ is a precomputed scalar.

For the alternative method of evaluating $D$, as discussed in part 1 of this exercise, we require:

**a.** $(p + 1)$ multiplies and adds to give the product $\hat{r}(k)r_a(k)$ for $1 \leq k \leq p$ and to give $\hat{r}(0)r_a(0)$.

**b.** 1 divide to give $D$ since $\hat{\mathbf{a}}' \mathbf{R}_{\hat{x}} \hat{\mathbf{a}}$ is a precomputed scalar.

Thus, neglecting the divide, the alternative computation of $D$ requires a factor of $(p+2)$ less computation and therefore is significantly more efficient than direct computation of the ratio of prediction residuals.

### 3.3.9 Typical LPC Analysis Parameters

The computation of the LPC analysis system of Figure 3.37 is specified by a number of variable parameters, including

Amazon / Zentian Limited
Exhibit 1013
Page 152

$N$ number of samples in the analysis frame

$M$ number of samples shift between frames

$p$ LPC analysis order

$Q$ dimension of LPC derived cepstral vector

$K$ number of frames over which cepstral time derivatives are computed.

Although each of these parameters can be varied over a wide range of values, the following table gives typical values for analysis systems at three different sampling rates (6.67 kHz, 8 kHz, 10 kHz).

Typical Values of LPC Analysis Parameters for Speech-Recognition Systems

| parameter | $F_s = 6.67$ kHz | | $F_s = 8$ kHz | | $F_s = 10$ kHz | |
|---|---|---|---|---|---|---|
| $N$ | 300 | (45 msec) | 240 | (30 msec) | 300 | (30 msec) |
| $M$ | 100 | (15 msec) | 80 | (10 msec) | 100 | (10 msec) |
| $p$ | 8 | | 10 | | 10 | |
| $Q$ | 12 | | 12 | | 12 | |
| $K$ | 3 | | 3 | | 3 | |

## 3.4 VECTOR QUANTIZATION

The results of either the filter-bank analysis or the LPC analysis are a series of vectors characteristic of the time-varying spectral characteristics of the speech signal. For convenience, we denote the spectral vectors as $\mathbf{v}_\ell$, $\ell = 1, 2, \ldots, L$, where typically each vector is a $p$-dimensional vector. If we compare the information rate of the vector representation to that of the raw (uncoded) speech waveform, we see that the spectral analysis has significantly reduced the required information rate. Consider, for example, 10-kHz sampled speech with 16-bit speech amplitudes. A raw signal information rate of 160,000 bps is required to store the speech samples in uncompressed format. For the spectral analysis, consider vectors of dimension $p = 10$ using 100 spectral vectors per second. If we again represent each spectral component to 16-bit precision, the required storage is about $100 \times 10 \times 16$ bps, or 16,000 bps—about a 10-to-1 reduction over the uncompressed signal. Such compressions in storage rate are impressive. Based on the concept of ultimately needing only a single spectral representation for each basic speech unit, it may be possible to further reduce the raw spectral representation of speech to those drawn from a small, finite number of "unique" spectral vectors, each corresponding to one of the basic speech units (i.e., the phonemes). This ideal representation is, of course, impractical, because there is so much variability in the spectral properties of each of the basic speech units. However, the concept of building a codebook of "distinct" analysis vectors, albeit with significantly more code words than the basic set of phonemes, remains an attractive idea and is the basis behind a set of techniques commonly called vector quantization (VQ) methods. Based on this line of reasoning, assume that we require a codebook with about 1024 unique spectral vectors

Amazon / Zentian Limited
Exhibit 1013
Page 153

(i.e., about 25 variants for each of the 40 basic speech units). Then to represent an arbitrary spectral vector all we need is a 10-bit number—the index of the codebook vector that best matches the input vector. Assuming a rate of 100 spectral vectors per second, we see that a total bit rate of about 1000 bps is required to represent the spectral vectors of a speech signal. This rate is about $1/16^{th}$ the rate required by the continuous spectral vectors. Hence the VQ representation is potentially an extremely efficient representation of the spectral information in the speech signal. This is one of the main reasons for the interest in VQ methods.

Before discussing the concepts involved in designing and implementing a practical VQ system, we first discuss the advantages and disadvantages of this type of representation. The key advantages of the VQ representation are

- reduced storage for spectral analysis information. We have already shown that the VQ representation is potentially very efficient. This efficiency can be exploited in a number of ways in practical VQ-based speech-recognition systems.
- reduced computation for determining similarity of spectral analysis vectors. In speech recognition a major component of the computation is the determination of spectral similarity between a pair of vectors. Based on the VQ representation, this spectral similarity computation is often reduced to a table lookup of similarities between pairs of codebook vectors.
- discrete representation of speech sounds. By associating a phonetic label (or possibly a set of phonetic labels or a phonetic class) with each codebook vector, the process of choosing a best codebook vector to represent a given spectral vector becomes equivalent to assigning a phonetic label to each spectral frame of speech. A range of recognition systems exist that exploit these labels so as to recognize speech in an efficient manner.

The disadvantages of the use of a VQ codebook to represent speech spectral vectors are

- an inherent spectral distortion in representing the actual analysis vector. Since there is only a finite number of codebook vectors, the process of choosing the "best" representation of a given spectral vector inherently is equivalent to quantizing the vector and leads, by definition, to a certain level of quantization error. As the size of the codebook increases, the size of the quantization error decreases. However, with any finite codebook there will always be some nonzero level of quantization error.
- the storage required for codebook vectors is often nontrivial. The larger we make the codebook (so as to reduce quantization error), the more storage is required for the codebook entries. For codebook sizes of 1000 or larger, the storage is often nontrivial. Hence an inherent trade-off among quantization error, processing for choosing the codebook vector, and storage of codebook vectors exists, and practical designs balance each of these three factors.

### 3.4.1 Elements of a Vector Quantization Implementation

To build a VQ codebook and implement a VQ analysis procedure, we need the following:

Amazon / Zentian Limited
Exhibit 1013
Page 154

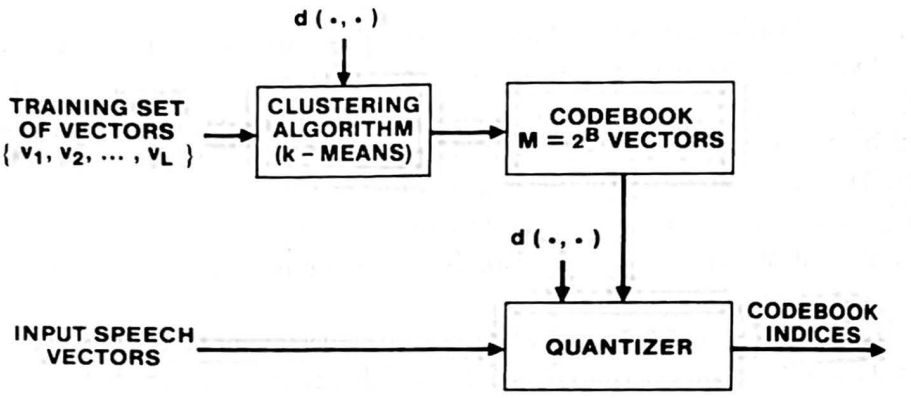



**Figure 3.40** Block diagram of the basic VQ training and classification structure.

1. a large set of spectral analysis vectors, $\mathbf{v}_1, \mathbf{v}_2, \ldots, \mathbf{v}_L$, which form a training set. The training set is used to create the "optimal" set of codebook vectors for representing the spectral variability observed in the training set. If we denote the size of the VQ codebook as $M = 2^B$ vectors (we call this a $B$-bit codebook), then we require $L \gg M$ so as to be able to find the best set of $M$ codebook vectors in a robust manner. In practice, it has been found that $L$ should be at least $10M$ in order to train a VQ codebook that works reasonably well.
2. a measure of similarity, or distance, between a pair of spectral analysis vectors so as to be able to cluster the training set vectors as well as to associate or classify arbitrary spectral vectors into unique codebook entries. We denote the spectral distance, $d(\mathbf{v}_i, \mathbf{v}_j)$, between two vectors $\mathbf{v}_i$ and $\mathbf{v}_j$ as $d_{ij}$. We defer a discussion of spectral distance measures to Chapter 4.
3. a centroid computation procedure. On the basis of the partitioning that classifies the $L$ training set vectors into $M$ clusters we choose the $M$ codebook vectors as the centroid of each of the $M$ clusters.
4. a classification procedure for arbitrary speech spectral analysis vectors that chooses the codebook vector closest to the input vector and uses the codebook index as the resulting spectral representation. This is often referred to as the nearest-neighbor labeling or optimal encoding procedure. The classification procedure is essentially a quantizer that accepts, as input, a speech spectral vector and provides, as output, the codebook index of the codebook vector that best matches the input.

Figure 3.40 shows a block diagram of the basic VQ training and classification structure. In the following sections we discuss each element of the VQ structure in more detail.

### 3.4.2 The VQ Training Set

To properly train the VQ codebook, the training set vectors should span the anticipated range of the following:

Amazon / Zentian Limited
Exhibit 1013
Page 155

- talkers, including ranges in age, accent, gender, speaking rate, levels, and other variables.
- speaking conditions, such as quiet room, automobile, and noisy workstation.
- transducers and transmission systems, including wideband microphones, telephone handsets (with both carbon and electret microphones), direct transmission, telephone channel, wideband channel, and other devices.
- speech units including specific-recognition vocabularies (e.g., digits) and conversational speech.

The more narrowly focused the training set (i.e., limited talker populations, quiet room speaking, carbon button telephone over a standard telephone channel, vocabulary of digits) the smaller the quantization error in representing the spectral information with a fixed-size codebook. However, for applicability to a wide range of problems, the training set should be as broad, in each of the above dimensions, as possible.

### 3.4.3 The Similarity or Distance Measure

The spectral distance measure for comparing spectral vectors $\mathbf{v}_i$ and $\mathbf{v}_j$ is of the form

$$d(\mathbf{v}_i, \mathbf{v}_j) = d_{ij} \begin{cases} = 0 & \text{if } \mathbf{v}_i = \mathbf{v}_j \\ > 0 & \text{otherwise} \end{cases} . \tag{3.93}$$

As we will see in Chapter 4, the distance measure commonly used for comparing filter-bank vectors is an $L_1$, $L_2$, or covariance weighted spectral difference, whereas for LPC vectors (and related feature sets such as LPC derived cepstral vectors), measures such as the likelihood and cepstral distance measures are generally used.

### 3.4.4 Clustering the Training Vectors

The way in which a set of $L$ training vectors can be clustered into a set of $M$ codebook vectors is the following (this procedure is known as the generalized Lloyd algorithm or the $K$-means clustering algorithm):

1. Initialization: Arbitrarily choose $M$ vectors (initially out of the training set of $L$ vectors) as the initial set of code words in the codebook.
2. Nearest-Neighbor Search: For each training vector, find the code word in the current codebook that is closest (in terms of spectral distance), and assign that vector to the corresponding cell (associated with the closest code word).
3. Centroid Update: Update the code word in each cell using the centroid of the training vectors assigned to that cell.
4. Iteration: Repeat steps 2 and 3 until the average distance falls below a preset threshold.

Figure 3.41 illustrates the result of designing a VQ codebook by showing the partitioning of a (2-dimensional) spectral vector space into distinct regions, each of which is

Amazon / Zentian Limited
Exhibit 1013
Page 156

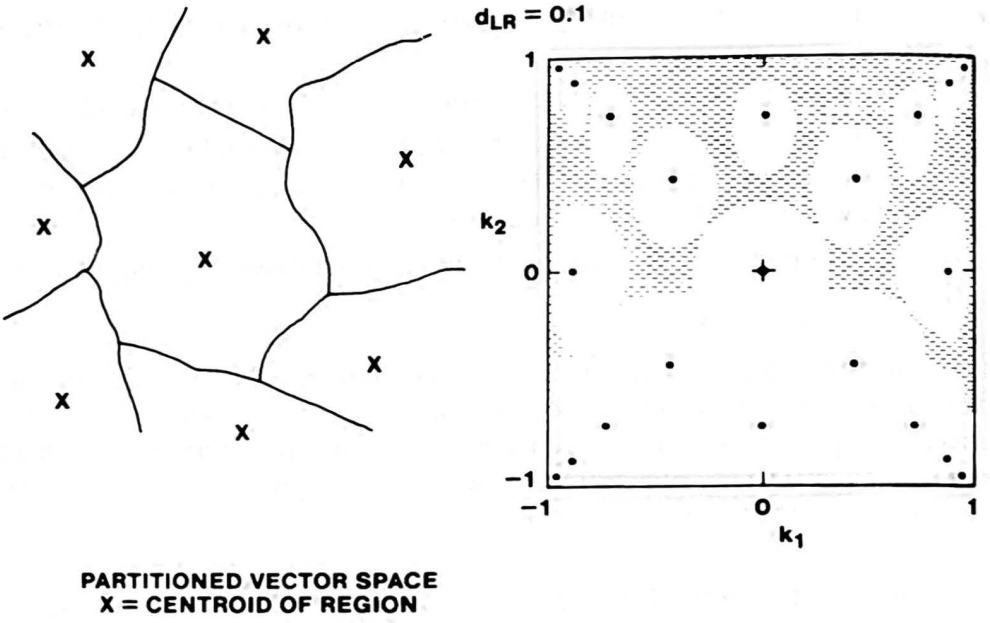



**Figure 3.41** Partitioning of a vector space into VQ cells with each cell represented by a centroid vector.

represented by a centroid vector. The shape of each partitioned cell is highly dependent on the spectral distortion measure and the statistics of the vectors in the training set. (For example, if a Euclidean distance is used, the cell boundaries are hyperplanes.)

Although the above iterative procedure works well, it has been shown that it is advantageous to design an $M$-vector codebook in stages—i.e., by first designing a 1-vector codebook, then using a splitting technique on the code words to initialize the search for a 2-vector codebook, and continuing the splitting process until the desired $M$-vector codebook is obtained. This procedure is called the binary split algorithm and is formally implemented by the following procedure:

1. Design a 1-vector codebook; this is the centroid of the entire set of training vectors (hence, no iteration is required here).
2. Double the size of the codebook by splitting each current codebook $\mathbf{y}_n$ according to the rule

$$\begin{aligned} \mathbf{y}_n^+ &= \mathbf{y}_n(1+\epsilon) \\ \mathbf{y}_n^- &= \mathbf{y}_n(1-\epsilon), \end{aligned} \tag{3.94}$$

   where $n$ varies from 1 to the current size of the codebook, and $\epsilon$ is a splitting parameter (typically $\epsilon$ is chosen in the range $0.01 \leq \epsilon \leq 0.05$).
3. Use the $K$-means iterative algorithm (as discussed above) to get the best set of centroids for the split codebook (i.e., the codebook of twice the size).
4. Iterate steps 2 and 3 until a codebook of size $M$ is designed.

Amazon / Zentian Limited
Exhibit 1013
Page 157

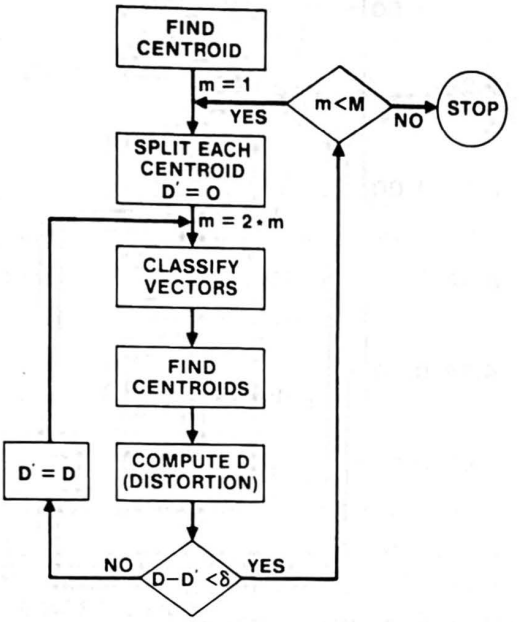



**Figure 3.42** Flow diagram of binary split codebook generation algorithm.

Figure 3.42 shows, in a flow diagram, the detailed steps of the binary split VQ codebook generation technique. The box labeled "Classify Vectors" is the nearest-neighbor search procedure, and the box labeled "Find Centroids" is the centroid update procedure of the $K$-means algorithm. The box labeled "Compute $D$ (Distortion)" sums the distances of all training vectors in the nearest-neighbor search so as to determine whether the procedure has converged (i.e., $D = D'$ of the previous iteration).

To illustrate the effect of codebook size (i.e., number of codebook vectors) on average training set distortion, Figure 3.43 [12] shows experimentally measured values of distortion (in terms of the likelihood ratio measure and the equivalent dB values; see Chapter 4 for more details) versus codebook size (as measured in bits per frame, $B$) for vectors of both voiced and unvoiced speech. It can be seen that very significant reductions in distortion are achieved in going from a codebook size of 1 bit (2 vectors) to about 7 bits (128 vectors) for both voiced and unvoiced speech. Beyond this point, reductions in distortion are much smaller.

One initial motivation for considering the use of a VQ codebook was the assumption that, in the limit, the codebook should ideally have about 40 vectors—i.e., one vector per speech sound. However, since the codebook vectors represent short time spectral measurements, there is inherently a certain degree of variability in specific codebook entries. Figure 3.44 shows a comparison of codebook vector locations in the $F_1 - F_2$ plane for a 32-vector codebook, along with the vowel ellipses discussed in Chapter 2. (The 32 codewords were generated from a training set of conversational speech spoken by a set of male talkers. The training set included both speech and background signals.) It can be seen that the correspondence between codebook vector location and vowel location is weak. Furthermore, there appears to be a tendency to cluster around the neutral vowel /ɜ/.

Amazon / Zentian Limited
Exhibit 1013
Page 158

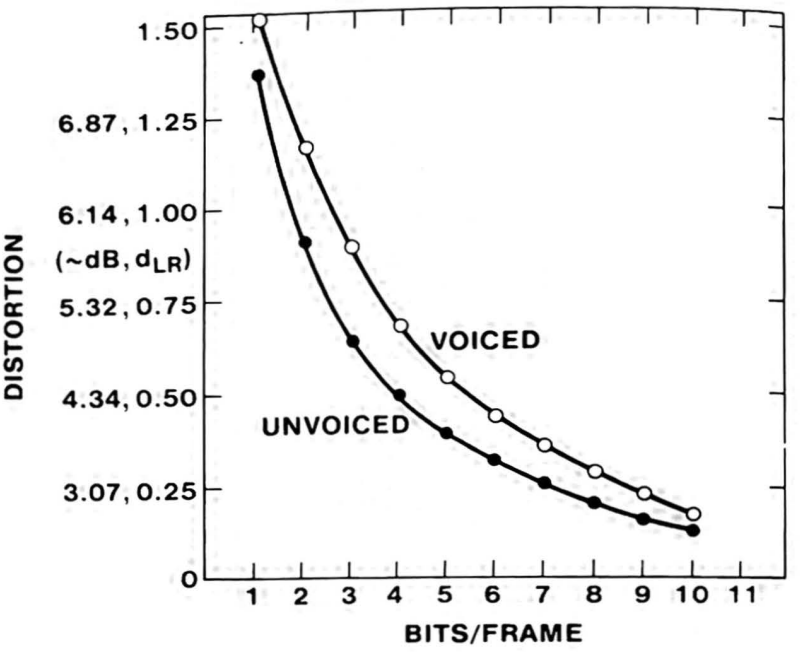



**Figure 3.43** Codebook distortion versus codebook size (measured in bits per frame) for both voiced and unvoiced speech (after Juang et al. [12]).

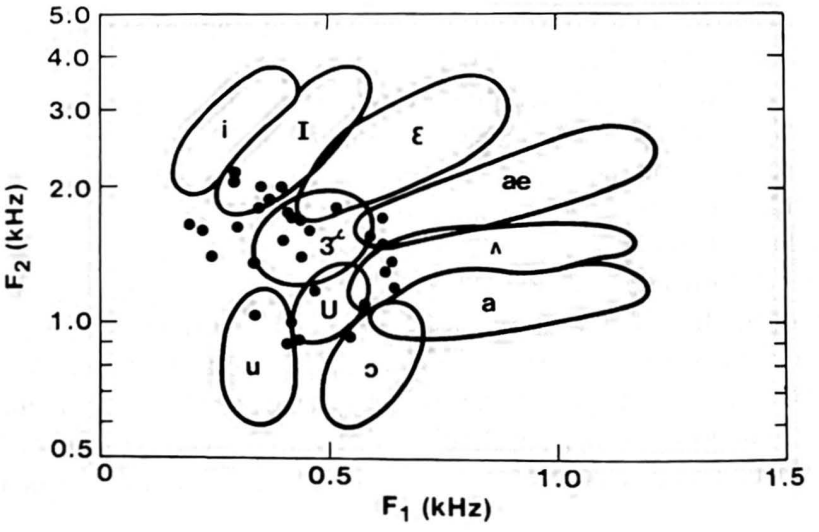



**Figure 3.44** Codebook vector locations in the $F_1 - F_2$ plane (for a 32-vector codebook) superimposed on the vowel ellipses (after Juang et al. [12]).

This can be attributed, in part, to both the distortion measure and to the manner in which spectral centroids are computed.

### 3.4.5 Vector Classification Procedure

The classification procedure for arbitrary spectral vectors is basically a full search through the codebook to find the "best" match. Thus if we denote the codebook vectors of an

Amazon / Zentian Limited
Exhibit 1013
Page 159

$M$-vector codebook as $\mathbf{y}_m$, $1 \leq m \leq M$, and we denote the spectral vector to be classified (and quantized) as $\mathbf{v}$, then the index, $m^*$, of the best codebook entry is

$$m^* = \arg \min_{1 \leq m \leq M} d(\mathbf{v}, \mathbf{y}_m). \tag{3.95}$$

For codebooks with large values of $M$ (e.g., $M \geq 1024$), the computation of Eq. (3.95) could be excessive, depending on the exact details of the distance measure; hence, alternative, suboptimal, procedures for designing VQ codebooks have been investigated. We will briefly discuss such methods in a later section of this chapter.

### 3.4.6 Comparison of Vector and Scalar Quantizers

To illustrate the power of the concept of quantizing an entire vector (rather than quantizing individual components of the vector), Figures 3.45 and 3.46 show comparisons of the results of using vector and scalar quantizers on typical speech spectral frames. In Figure 3.45 we see both model (speech) spectra and the resulting quantization error spectrum for 10-bit and 24-bit scalar quantizers and for a 10-bit vector quantizer. It is clear that the quantization error of the 10-bit vector quantizer is comparable to that of the 24-bit scalar quantizer. This implies that the vector quantizer provides a 14-bit reduction in storage (per frame) over a scalar quantizer, i.e., more than a 50% reduction in storage for the same distortion.

Figure 3.46 shows temporal plots of distortion as well as distortion error histograms for the three quantizers of Figure 3.45. It can be seen that even though the average distortion of the 10-bit VQ is comparable to that of the 24-bit scalar quantizer, the peak distortion of the 10-bit VQ is much smaller than the peak distortion of the 24-bit scalar quantizer. This represents another distinct advantage of VQ over scalar quantization.

### 3.4.7 Extensions of Vector Quantization

As mentioned earlier, several straightforward extensions of the ideas of VQ have been proposed and studied, including the following:

1. Use of multiple codebooks in which codebooks are created separately (and independently) for each of several spectral (or temporal) representations of speech. Thus we might consider using a separate codebook for cepstral vectors and a separate codebook for the time derivatives of the cepstral vectors. This method of multiple codebooks has been used extensively in large vocabulary speech-recognition systems.
2. Binary search trees in which a series of suboptimal VQs is used to limit the search space so as to reduce the computation of the overall VQ from $M$ distances to log ($M$) distances. The training procedure first designs an optimal $M = 2$ VQ and then assigns all training vectors to one of the VQ cells. Next the procedure designs a pair of $M = 2$ VQs, one for each subset of the preceding stage. This process is iterated until the desired size is obtained in log $M$ steps. The suboptimality of the procedure is related to the fact that training vectors initially split along one branch of the VQ cannot join the other branch at a later stage of processing; hence, the overall

Amazon / Zentian Limited
Exhibit 1013
Page 160

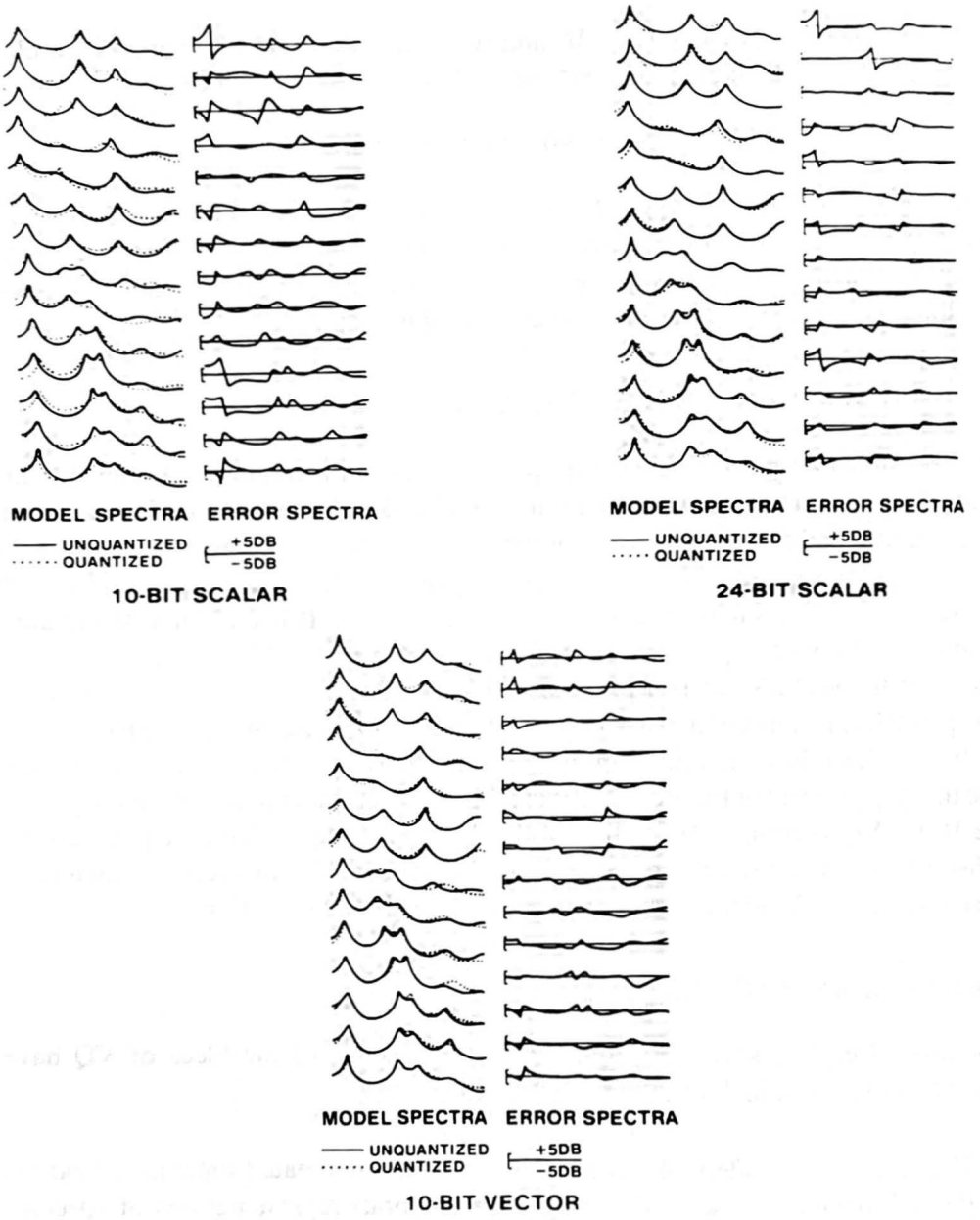



**Figure 3.45** Model and distortion error spectra for scalar and vector quantizers (after Juang et al. [12]).

distortion is not minimal at each branch of the tree.

3. $K$-tuple (fixed-length block) quantizers in which $K$-frames of speech are coded at a time, rather than single frames, as is conventionally the case. The idea is to exploit correlations in time for vowels and vowel-like sounds. The disadvantage occurs for sounds where the correlation along the $K$-tuple is low—i.e., transient sounds and many consonants.
4. Matrix quantization in which a codebook of sounds or words of variable sequence

Amazon / Zentian Limited
Exhibit 1013
Page 161

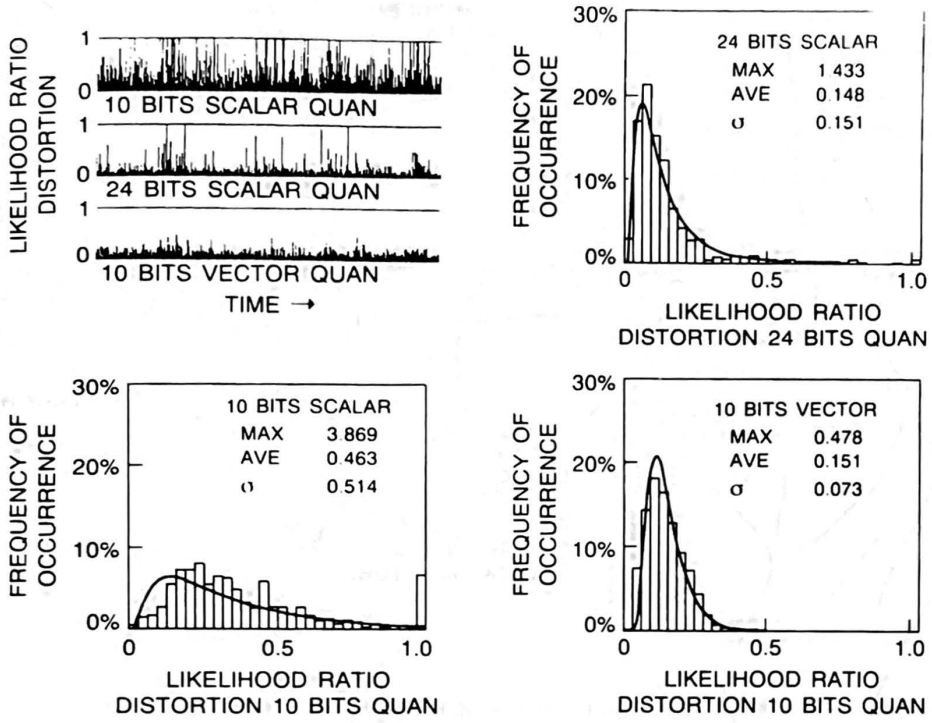



**Figure 3.46** Plots and histograms of temporal distortion for scalar and vector quantizers (after Juang et al. [12]).

length is created. The concept here is to handle time variability via some types of dynamic programming procedure and thereby create a codebook of sequences of vectors that represent typical sounds or words. Such techniques are most applicable to word-recognition systems.

5. Trellis codes in which time sequential dependencies among codebook entries are explicitly determined as part of the training phase. The idea here is that when input vector $\mathbf{v}_n$ is quantized using codeword $\mathbf{y}_\ell$, then input vector $\mathbf{v}_{n+1}$ is quantized using one of a limited subset of codebook entries that are related to $\mathbf{y}_\ell$ via a set of learned sequential constraints, thereby reducing computation of encoding the input, and increasing the ability to interpret the codebook output in terms of basic speech units.
6. Hidden Markov models in which both time and spectral constraints are used to quantize an entire speech utterance in a well-defined and efficient manner. We defer a discussion of hidden Markov models to Chapter 6.

### 3.4.8 Summary of the VQ Method

In later chapters of this book we will see several examples of how VQ concepts can be exploited in speech-recognition systems. Here we have shown that the basic idea of VQ is to reduce the information rate of the speech signal to a low rate through the use of a codebook with a relatively small number of code words. The goal is to be able to

Amazon / Zentian Limited
Exhibit 1013
Page 162

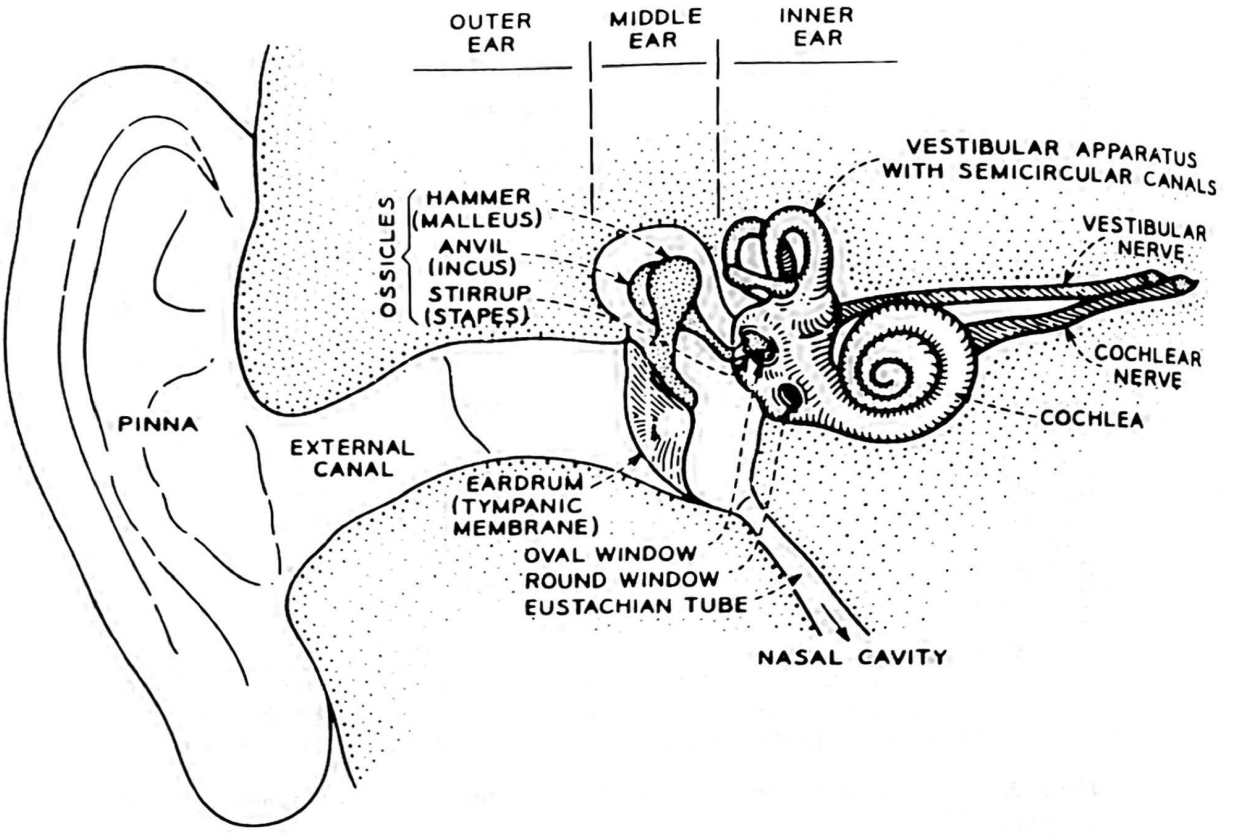



**Figure 3.47** Physiological model of the human ear.

represent the spectral information of the signal in an efficient manner and in a way that direct connections to the acoustic-phonetic framework discussed in Chapter 2 can be made. Various techniques for achieving this efficiency of representation were discussed, and their properties were illustrated on representative examples of speech.

## 3.5 AUDITORY-BASED SPECTRAL ANALYSIS MODELS

The motivation for investigating spectral analysis methods that are physiologically based is to gain an understanding of how the human auditory system processes speech, so as to be able to design and implement robust, efficient methods of analyzing and representing speech. It is generally assumed that the better we understand the signal processing in the human auditory system, the closer we will come to being able to design a system that can truly understand meaning as well as content of speech.

With these considerations in mind, we first examine a physiological model of the human ear. Such a model is given in Figure 3.47 and it shows that the ear has three distinct regions called the outer ear, the middle ear, and the inner ear. The outer ear consists of the pinna (the ear surface surrounding the canal in which sound is funneled), and the external canal. Sound waves reach the ear and are guided through the outer ear to the

Amazon / Zentian Limited
Exhibit 1013
Page 163

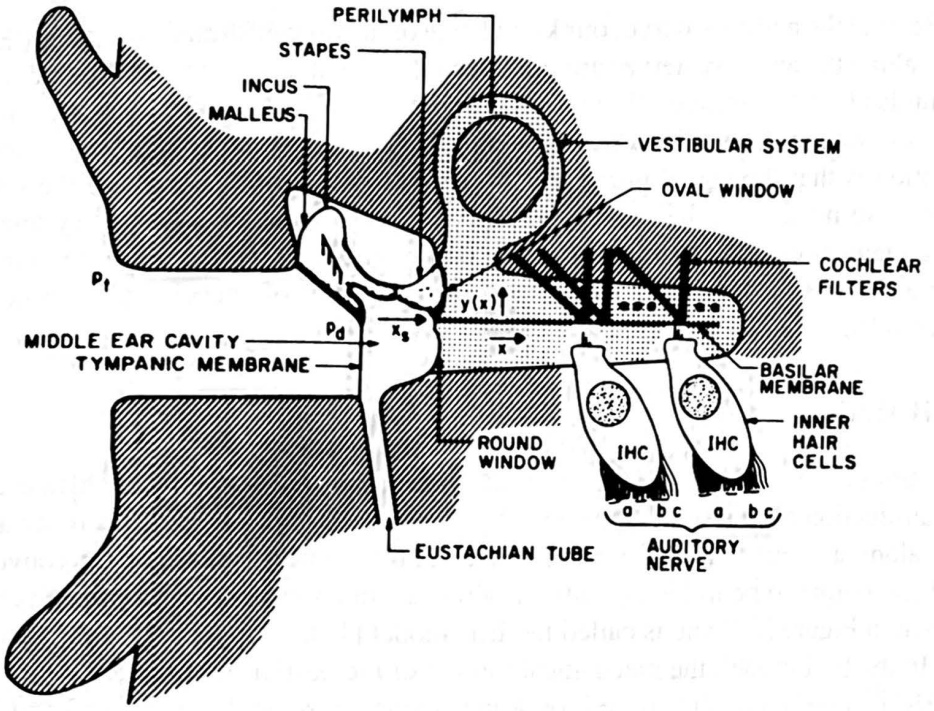



**Figure 3.48** Expanded view of the middle and inner ear mechanics.

middle ear, which consists of the tympanic membrane or eardrum upon which the sound wave impinges and causes to move and a mechanical transducer (the malleus or hammer, the incus or anvil, and the stapes or stirrup), which converts the acoustical sound wave to mechanical vibrations along the inner ear. The inner ear consists of the cochlea, which is a fluid-filled chamber partitioned by the basilar membrane, and the cochlea or auditory nerve. The mechanical vibrations impinging on the oval window at the entrance to the cochlea create standing waves (of the fluid inside the cochlea) that cause the basilar membrane to vibrate at frequencies commensurate with the input acoustic wave frequencies (e.g., the formants of voiced speech) and at a place along the basilar membrane that is associated with these frequencies. (An expanded view of the middle and inner ear mechanics is given in Figure 3.48. The $2\,^1/_2$ turn, snail-like shape of the cochlea is shown as a straight tube in this figure for ease of presentation.)

The basilar membrane is characterized by a set of frequency responses at different points along the membrane. Hence, in its simplest form, the cochlea can be modeled as a mechanical realization of a bank of filters (appropriately called cochlea filters). Distributed along the basilar member (in a dense but discrete manner) is a set of sensors called inner hair cells (IHC), which act as mechanical motion to neural activity converters. Mechanical motion at some point along the basilar membrane is sensed by the inner hair cells and causes firing activity at the nerve fibers that innervate the bottom of each IHC. Each IHC is connected to about 10 nerve fibers, each of different diameter and of different synaptic connection. It has been shown experimentally that thin fibers fire (emit neural impulses) only at high motion levels, whereas thick fibers fire at much lower motion levels. A total of about 30,000 nerve fibers link the IHCs to the auditory nerve.

Amazon / Zentian Limited
Exhibit 1013
Page 164

Beyond the auditory nerve, our knowledge of how the information signals (the neural activity along the auditory nerve) are processed and eventually converted to intelligence in the brain is almost primitive. Hence when we attempt to build auditory models for signal processing, we are primarily modeling the middle ear, cochlea, and hair cell systems. The assumption is that the signal produced by such a model exhibits some of the robustness (immunity to noise, reverberation) and efficiency of the human auditory systems. Thus in the remainder of this section we present one such model, called the Ensemble Interval Histogram (EIH) model and show some of the properties of speech signals processed by such a model.

### 3.5.1 The EIH Model

On the basis of the discussion in the preceding section, a model of the cochlea and the hair cell transduction consists of a filter bank that models the frequency selectivity at various points along a simulated basilar membrane, and a nonlinear processor for converting the filter bank output to neural firing patterns along a simulated auditory nerve. Such a model is shown in Figure 3.49 and is called the EIH model [13].

In the EIH model, the mechanical motion of the basilar membrane is sampled using 165 IHC channels, equally spaced, on a log-frequency scale, between 150 and 7000 Hz. The corresponding cochlear filters are based on actual neural tuning curves for cats. The amplitude responses of 28 of these filters (i.e., about 1 in 8 from the model) are shown in Figure 3.50. The phase characteristics of these filters is minimum phase, and the relative gain, measured at the center frequency of the filter, reflects the corresponding value of the cat's middle ear transfer function.

The next stage of processing in the EIH model of Figure 3.49 is an array of level crossing detectors that models the motion-to-neural activity transduction of the hair cell mechanisms. The detection levels of each detector are pseudo-randomly distributed (based on measured distributions of level firings), thereby simulating the variability of fiber diameters and their synaptic connections.

The output of the level-crossing detectors represents the discharge activity of the auditory nerve fibers. Figure 3.51 shows simulated auditory nerve activity, for the first 60 msec of the vowel /o/ in the word "job," as a function of both time and the "characteristic frequency" of the IHC channels. (Note the logarithmic scale of the characteristic frequency which represents the place-to-frequency mapping on the basilar membrane.) In Figure 3.51, a level-crossing occurrence is marked as a single dot, and the output activity of each level-crossing detector is plotted as a separate trace. Each IHC channel contributes seven parallel traces (corresponding to the seven level-crossing detectors for each channel), with the lowest trace representing the lowest-threshold level-crossing detector. If the magnitude of the filter's output is low, only one level will be crossed, as is seen for the very top channels in Figure 3.51. However, for large signal magnitudes, several levels will be activated, creating a "darker" area of activity in the figure.

The level-crossing patterns represent the auditory nerve activity, which, in turn, is the input to a second, more central stage of neural processing, which gives the overall ensemble interval histogram (EIH). Conceptually, the EIH is a measure of the spatial

Amazon / Zentian Limited
Exhibit 1013
Page 165

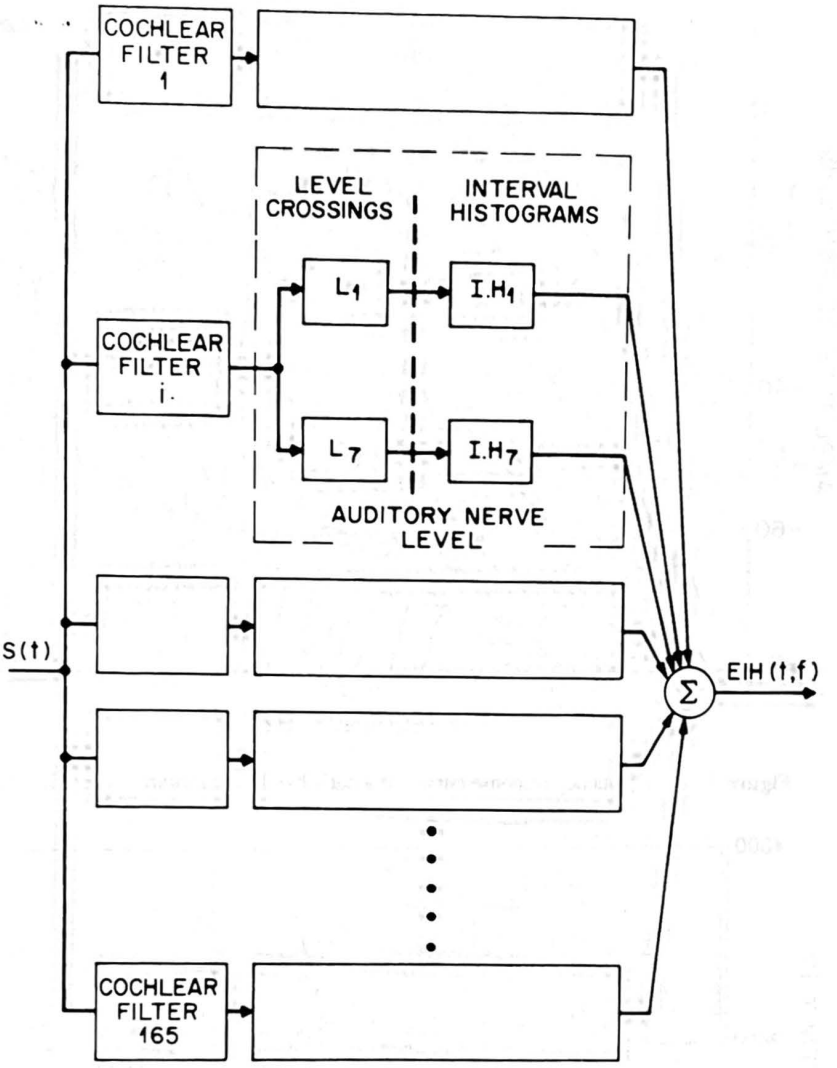



**Figure 3.49** Block diagram of the EIH model (after Ghitza [13]).

extent of coherent neural activity across the simulated auditory nerve. Mathematically, it is the short-term probability density function of the reciprocal of the intervals between successive firings, measured over the entire simulated auditory nerve in a characteristic frequency-dependent time-frequency zone.

As a consequence of the multilevel crossing detectors, the EIH representation preserves information about the signal's overall energy. To illustrate this point, consider the case in which the input signal is a pure sinusoid, i.e. $s(t) = A\sin(2\pi f_0 t)$, and the characteristic frequency of a selected channel is $f_0$, as shown in Figure 3.52a. For a given intensity $A$, the cochlear filter output will activate only some low level-crossing detectors. For a given detector, the time interval between two successive positive-going level crossings is $1/f_0$. Since the histogram is scaled in units of frequency, this interval contributes a count to the $f_0$ bin. For the input signal in Figure 3.52a, all of the intervals are the same, resulting in a histogram in which the magnitude of each bin, save one ($f_0$), is zero. As the signal

Amazon / Zentian Limited
Exhibit 1013
Page 166

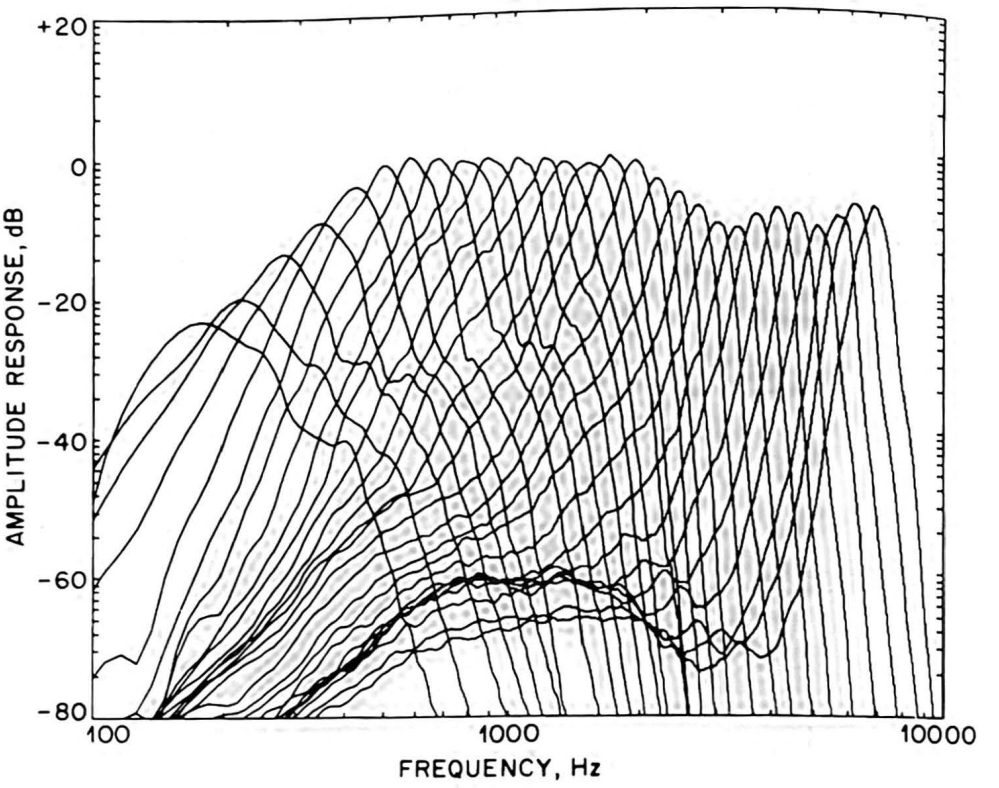



**Figure 3.50** Frequency response curves of a cat's basilar membrane (after Ghitza [13]).

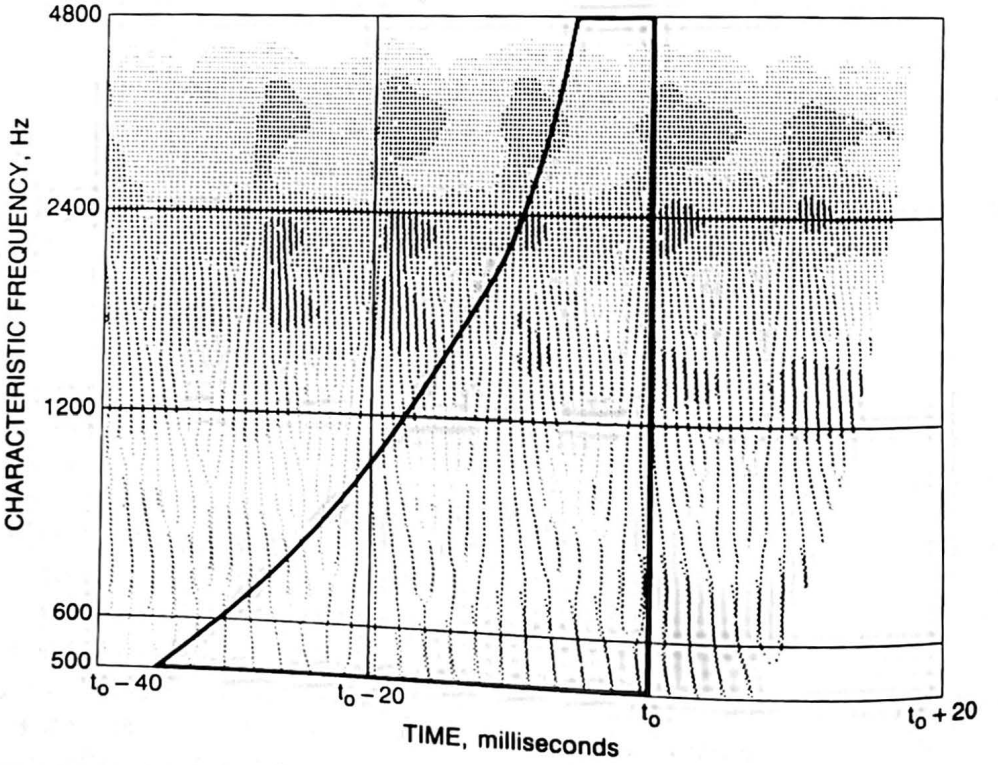



**Figure 3.51** Magnitude of EIH for vowel /o/ showing the time-frequency resolution (after Ghitza [13]).

Amazon / Zentian Limited
Exhibit 1013
Page 167

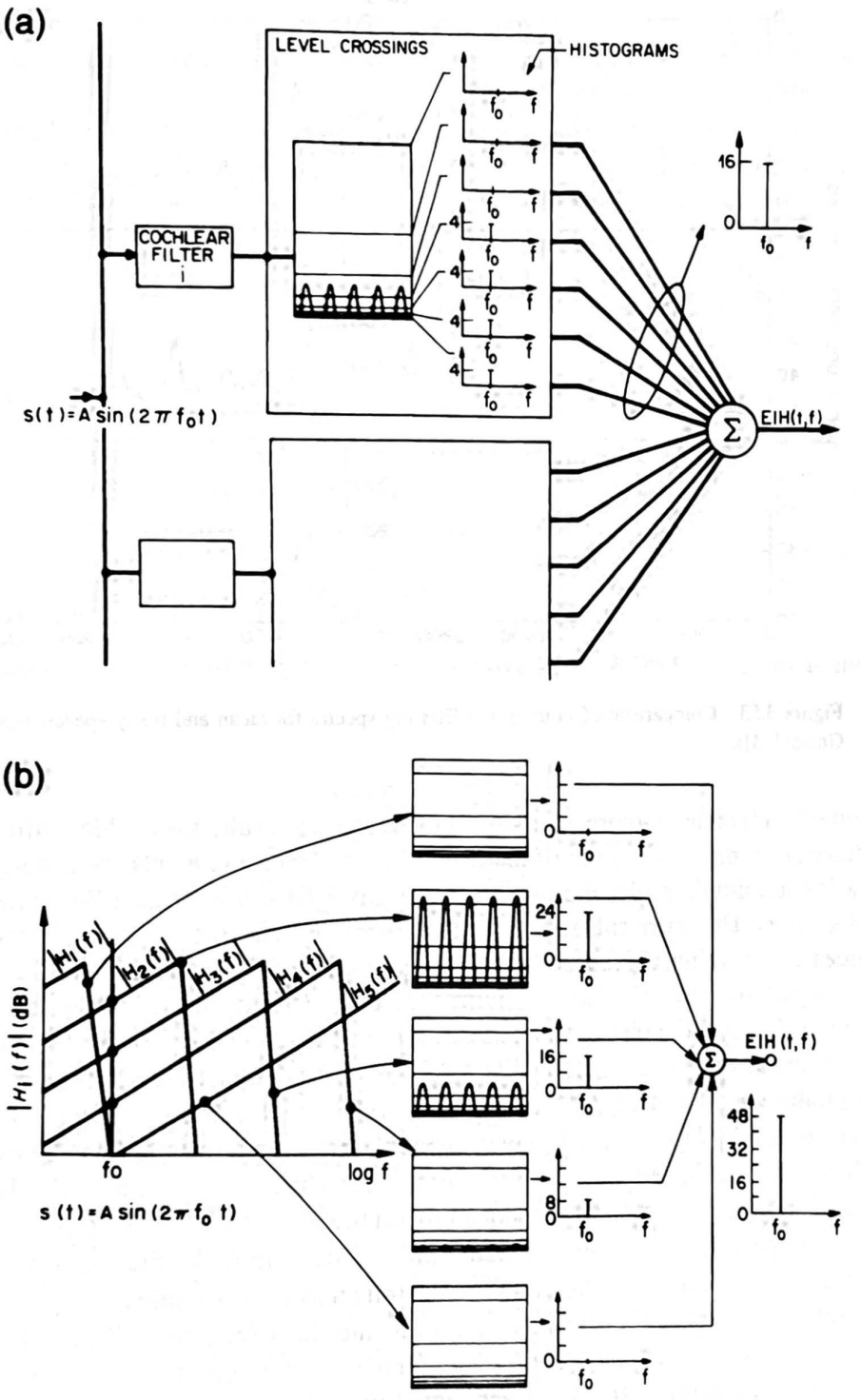



**Figure 3.52** Operation of the EIH model for a pure sinusoid (after Ghitza [13]).

Amazon / Zentian Limited
Exhibit 1013
Page 168

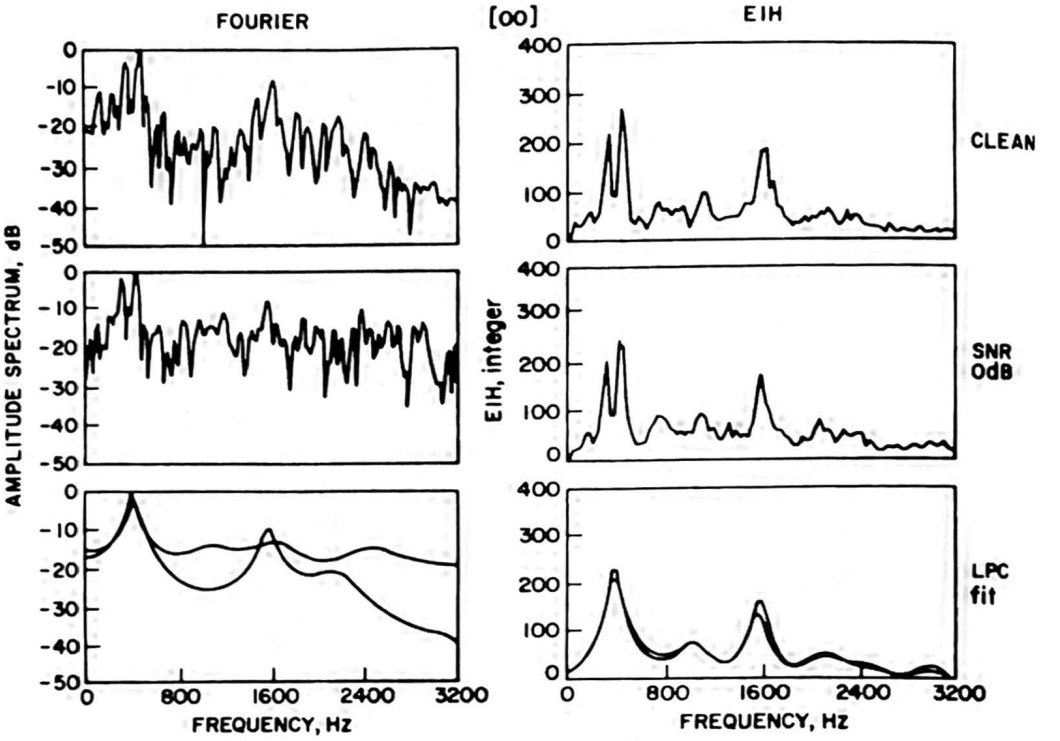



**Figure 3.53** Comparison of Fourier and EIH log spectra for clean and noisy speech signals (after Ghitza [13]).

amplitude $A$ increases, more levels are activated. As a result, this cochlear filter contributes additional counts to the $f_0$ bin of the EIH. Since the crossing levels are equally distributed on a log-amplitude scale, the magnitude of any EIH bin is related, in some fashion, to decibel units. However, this relation is not a straightforward one because there are several sources contributing counts to the $f_0$ bin in a nonlinear manner. Figure 3.52b shows an input signal $s(t) = A\sin(2\pi f_0 t)$ driving five adjacent cochlear filters with an amplitude response $|H_i(f)|$ and a phase response $\phi_i(f)$, $i = 1, 2, \ldots, 5$. Due to the shape of the filters, more than one cochlear channel will contribute to the $f_0$ bin. In fact, all the cochlear filters that produce $s_i(t) = A\,|H_i(f_0)|\sin(2\pi f_0 t + \phi_i(f_0))$ will contribute to the $f_0$ bin of the EIH, provided that $A\,|H_i(f_0)|$ exceeds any of the level-crossing thresholds. In Figure 3.52b only cochlear filters 2, 3, and 4 are contributing nonzero histograms to the EIH. The number of counts is different for each filter, depending on the magnitude of $A\,|H_i(f_0)|$.

One goal of auditory-based signal processing is to make the signal more robust to noise and reverberation than alternative spectral analysis procedures such as the filter-bank method or the LPC method. Figure 3.53 illustrates how well the EIH model achieves this goal. Shown in the figure are the log magnitude spectra of a clean (no noise) and a noisy (signal-to-noise ratio of 0 dB) speech signal processed by a standard Fourier filter bank (curves on the left) and by the EIH model (curves on the right). Also shown are LPC polynomial fits to the original signal spectrum (on the left) and to the EIH signal spectrum (on the right) for both the clean signal and the noisy signal. This figure clearly shows a tremendous sensitivity of the Fourier and LPC analyses to noise for the original signals.

Amazon / Zentian Limited
Exhibit 1013
Page 169

(This is especially seen in the LPC polynomial fits.) In the EIH case, the log magnitude spectra are almost unaltered by the noise, and the LPC polynomial fits are extremely close to each other.

The implication of the above results for speech recognition is that the EIH model has potential for use in recognizing speech robustly in noisy and reverberant environments. We will explore this issue in Chapter 5 when we talk about the effects of noise on performance of speech recognizers.

## 3.6 SUMMARY

In this chapter we have discussed several ways of performing spectral analysis of speech, including filter-bank analysis, LPC analysis, vector quantization, and auditory modeling. We have discussed the relative strengths and weaknesses of each approach and given a hint of the advantages and disadvantages for application to actual speech-recognition systems. We will see, in later chapters, how the type of spectral analysis that is used interacts with the processing of other parts of the recognizer. Only through such an understanding can one fully see the trade-offs among the different approaches to speech spectrum analysis.

## REFERENCES

[1] L.R. Rabiner and B. Gold, *Theory and Application of Digital Signal Processing*, Prentice Hall, Englewood Cliffs, NJ, 1975.

[2] L.R. Rabiner and R.W. Schafer, *Digital Processing of Speech Signals*, Prentice Hall, Englewood Cliffs, NJ, 1978.

[3] R.E. Crochiere and L.R. Rabiner, *Multirate Digital Signal Processing*, Prentice Hall, Englewood Cliffs, NJ, 1983.

[4] B.A. Dautrich, L.R. Rabiner, and T.B. Martin, "On the Effects of Varying Filter Bank Parameters on Isolated Word Recognition," *IEEE Trans. Acoustics, Speech, Signal Proc.*, ASSP-31 (4): 793–807, August 1983.

[5] B.A. Dautrich, L.R. Rabiner, and T.B. Martin, "The Effects of Selected Signal Processing Techniques on the Performance of a Filter Bank Based Isolated Word Recognizer," *Bell System Tech. J.*, 62 (5): 1311–1336, May–June 1983.

[6] J.D. Markel and A.H. Gray, Jr., *Linear Prediction of Speech*, Springer-Verlag, 1976.

[7] G.M. White and R.B. Neely, "Speech Recognition Experiments with Linear Prediction, Bandpass Filtering, and Dynamic Programming," *IEEE Trans. Acoustics, Speech, Signal Proc.*, ASSP-24 (2): 183–188, 1976.

[8] L.R. Rabiner, B.S. Atal, and M.R. Sambur, "LPC Prediction Error—Analysis of its Variation with the Position of the Analysis Frame," *IEEE Trans. Acoustics, Speech, Signal Proc.*, ASSP-25 (5): 434–442, October 1977.

[9] H. Strube, "Determination of the Instant of Glottal Closure from the Speech Wave," *J. Acoust. Soc. Am.*, 56 (5): 1625–1629, November 1974.

Amazon / Zentian Limited
Exhibit 1013
Page 170

[10] B.S. Atal and S.L. Hanauer, "Speech Analysis and Synthesis by Linear Prediction of the Speech Wave," *J. Acoust. Soc. Am.*, 50 (2): 637–655, August 1971.

[11] S. Furui, "Speaker Independent Isolated Word Recognition Using Dynamic Features of Speech Spectrum," *IEEE Trans. Acoustics, Speech, Signal Proc.*, ASSP-34 (1): 52-59, February 1986.

[12] J.-H. Juang, D.Y. Wong, and A.H. Gray, Jr., "Distortion Performance of Vector Quantization for LPC Voice Coding," *IEEE Trans. Acoustics, Speech, Signal Proc.*, ASSP-30 (2): 294–304, April 1982.

[13] O. Ghitza, "Auditory Nerve Representation as a Basis for Speech Processing," in *Advances in Speech Signal Processing*, S. Furui and M. Sondhi, Eds., Marcel Dekker, NY, 453–485, 1991.

Amazon / Zentian Limited
Exhibit 1013
Page 171

Chapter 6

# THEORY AND IMPLEMENTATION OF HIDDEN MARKOV MODELS

## 6.1 INTRODUCTION

In Chapters 4 and 5 we presented one major pattern-recognition approach to speech recognition, namely the template method. One key idea in the template method is to derive typical sequences of speech frames for a pattern (e.g., a word) via some averaging procedure, and to rely on the use of local spectral distance measures to compare patterns. Another key idea is to use some form of dynamic programming to temporally align patterns to account for differences in speaking rates across talkers as well as across repetitions of the word by the same talker. The methodology of the template approach is well developed and provides good recognition performance for a variety of practical applications.

The template approach, however, is not based on the ideas of statistical signal modeling in a strict sense. Even though statistical techniques have been widely used in clustering to create reference patterns, the template approach is best classified as a simplified, nonparametric method in which a multiplicity of reference tokens (sequences) are used to characterize the variation among different utterances. As such, statistical signal characterization inherent in the template representation is only implicit and often inadequate. Consider, for example, the use of a truncated cepstral distortion measure as the local distance for template matching. The Euclidean distance form of the cepstral distance measure suggests that the reference vector can be viewed as the *mean* of some assumed distribution.



Amazon / Zentian Limited
Exhibit 1013
Page 172

Obviously, this simple form of the sufficient statistic[1] (use of only the mean reference vector) neglects the second-order statistics—i.e., *covariances*, which, as will be seen later, are of particular significance in statistical modeling. (Note that this distribution is used to account for variations of the cepstral coefficients at the frame level since time alignment is performed so as to match appropriate frames of the patterns being compared.) There is clearly a need to use a more elaborate and analytical statistical method for speech recognition.

In this chapter we will study one well-known and widely used statistical method of characterizing the spectral properties of the frames of a pattern, namely the hidden Markov model (HMM) approach. (These models are also referred to as Markov sources or probabilistic functions of Markov chains in the communications literature.) The underlying assumption of the HMM (or any other type of statistical model) is that the speech signal can be well characterized as a parametric random process, and that the parameters of the stochastic process can be determined (estimated) in a precise, well-defined manner. We will show that the HMM method provides a natural and highly reliable way of recognizing speech for a wide range of applications and integrates well into systems incorporating both task syntax and semantics.

The basic theory of hidden Markov models was published in a series of classic papers by Baum and his colleagues ([1]–[5]) in the late 1960s and early 1970s and was implemented for speech-processing applications by Baker [6] at CMU, and by Jelinek and his colleagues at IBM ([7]–[13]) in the 1970s.

We begin this chapter with a review of the theory of Markov chains and then extend the ideas to HMMs using several simple examples. Based on the now-classical approach of Jack Ferguson of IDA (Institute for Defense Analyses), as introduced in lectures and in writing [14], we will focus our attention on the three fundamental problems for HMM design, namely: the evaluation of the probability (or likelihood) of a sequence of observations given a specific HMM; the determination of a best sequence of model states; and the adjustment of model parameters so as to best account for the observed signal. We will show that once these three fundamental problems are solved, we can readily apply HMMs to selected problems in speech recognition.

## 6.2 DISCRETE-TIME MARKOV PROCESSES

Consider a system that may be described at any time as being in one of a set of $N$ distinct states indexed by $\{1, 2, \ldots, N\}$ as illustrated in Figure 6.1 (where $N = 5$ for simplicity). At regularly spaced, discrete times, the system undergoes a change of state (possibly back to the same state) according to a set of probabilities associated with the state. We denote the time instants associated with state changes as $t = 1, 2, \ldots$, and we denote the actual

[1] Sufficient statistics are a set of measurements from a process which contain all the relevant information for estimating the parameters of that process.

Amazon / Zentian Limited
Exhibit 1013
Page 173

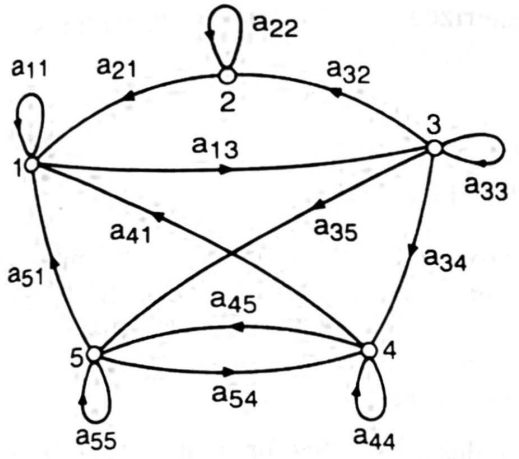



**Figure 6.1** A Markov chain with five states (labeled 1 to 5) with selected state transitions.

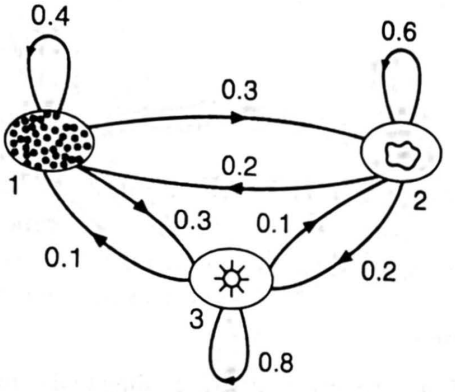



**Figure 6.2** Markov model of the weather.

state at time $t$ as $q_t$. A full probabilistic description of the above system would, in general, require specification of the current state (at time $t$), as well as all the predecessor states. For the special case of a discrete-time, first order, Markov chain, the probabilistic dependence is truncated to just the preceding state—that is,

$$P[q_t = j|q_{t-1} = i,\ q_{t-2} = k, \ldots] = P[q_t = j|q_{t-1} = i]. \tag{6.1}$$

Furthermore, we consider only those processes in which the right-hand side of (6.1) is independent of time, thereby leading to the set of state-transition probabilities $a_{ij}$ of the form

$$a_{ij} = P[q_t = j|q_{t-1} = i], \qquad 1 \leq i,j \leq N \tag{6.2}$$

with the following properties

$$a_{ij} \geq 0 \qquad \forall j, i \tag{6.3a}$$

$$\sum_{j=1}^{N} a_{ij} = 1 \qquad \forall i \tag{6.3b}$$

since they obey standard stochastic constraints.

The above stochastic process could be called an observable Markov model because the output of the process is the set of states at each instant of time, where each state corresponds to an observable event. To set ideas, consider a simple three-state Markov model of the weather as shown in Figure 6.2. We assume that once a day (e.g., at noon), the weather is observed as being one of the following:

**State 1:** precipitation (rain or snow)
**State 2:** cloudy
**State 3:** sunny.

Amazon / Zentian Limited
Exhibit 1013
Page 174

We postulate that the weather on day $t$ is characterized by a single one of the three states above, and that the matrix $A$ of state-transition probabilities is

$$A = \{a_{ij}\} = \begin{bmatrix} 0.4 & 0.3 & 0.3 \\ 0.2 & 0.6 & 0.2 \\ 0.1 & 0.1 & 0.8 \end{bmatrix}.$$

Given the model of Figure 6.2 we can now ask (and answer) several interesting questions about weather patterns over time. For example, we can pose the following simple problem:

**Problem**

What is the probability (according to the model) that the weather for eight consecutive days is "sun-sun-sun-rain-rain-sun-cloudy-sun"?

**Solution**

We define the observation sequence, **O**, as

| | | | | | | | | | |
|---|---|---|---|---|---|---|---|---|---|
| **O** | = | ( sunny, | sunny, | sunny, | rain, | rain, | sunny, | cloudy, | sunny ) |
| | = | ( 3, | 3, | 3, | 1, | 1, | 3, | 2, | 3 ) |
| day | | 1 | 2 | 3 | 4 | 5 | 6 | 7 | 8 |

corresponding to the postulated set of weather conditions over the eight-day period and we want to calculate $P(\mathbf{O}|\text{Model})$, the probability of the observation sequence **O**, given the model of Figure 6.2. We can directly determine $P(\mathbf{O}|\text{Model})$ as:

$$\begin{aligned} P(\mathbf{O}|\text{Model}) &= P[3, 3, 3, 1, 1, 3, 2, 3|\text{Model}] \\ &= P[3]\,P[3|3]^2 P[1|3]\,P[1|1] \\ &\quad P[3|1]\,P[2|3]\,P[3|2] \\ &= \pi_3 \cdot (a_{33})^2 a_{31}\, a_{11}\, a_{13}\, a_{32}\, a_{23} \\ &= (1.0)(0.8)^2(0.1)(0.4)(0.3)(0.1)(0.2) \\ &= 1.536 \times 10^{-4} \end{aligned}$$

where we use the notation:

$$\pi_i = P[q_1 = i], \qquad 1 \le i \le N \tag{6.4}$$

to denote the initial state probabilities.

Another interesting question we can ask (and answer using the model) is:

**Problem**

Given that the system is in a known state, what is the probability that it stays in that state for exactly

**Solution**

This probability can be evaluated as the probability of the observation sequence

| | | | | | | | |
|---|---|---|---|---|---|---|---|
| **O** | = ( $i$, | $i$, | $i$ | , . . . , | $i$, | $j \neq i$ ) |
| day | | 1 | 2 | 3 | | $d$ | $d+1$ |

Amazon / Zentian Limited
Exhibit 1013
Page 175

given the model, which is

$$\begin{aligned} P(\mathbf{O}|\text{Model}, q_1 = i) &= P(\mathbf{O}, q_1 = i|\text{Model})/P(q_1 = i) \\ &= \pi_i(a_{ii})^{d-1}(1 - a_{ii})/\pi_i \\ &= (a_{ii})^{d-1}(1 - a_{ii}) \\ &= p_i(d) \end{aligned} \tag{6.5}$$

The quantity $p_i(d)$ is the probability distribution function of duration $d$ in state $i$. This exponential distribution is characteristic of the state duration in a Markov chain. Based on $p_i(d)$, we can readily calculate the expected number of observations (duration) in a state, conditioned on starting in that state as

$$\bar{d}_i = \sum_{d=1}^{\infty} dp_i(d) \tag{6.6a}$$

$$= \sum_{d=1}^{\infty} d(a_{ii})^{d-1}(1 - a_{ii}) = \frac{1}{1 - a_{ii}}. \tag{6.6b}$$

Thus the expected number of consecutive days of sunny weather, according to the model, is $1/(0.2) = 5$; for cloudy it is 2.5; for rain it is 1.67.

**Problem**

Derive the expression for the mean of $p_i(d)$, i.e. Eq. (6.6b).

**Solution**

$$\begin{aligned} \bar{d}_i &= \sum_{d=1}^{\infty} dp_i(d) \\ &= \sum_{d=1}^{\infty} d(a_{ii})^{d-1}(1 - a_{ii}) \\ &= (1 - a_{ii})\frac{\partial}{\partial a_{ii}}\left[\sum_{d=1}^{\infty} a_{ii}^{d}\right] \\ &= (1 - a_{ii})\frac{\partial}{\partial a_{ii}}\left(\frac{a_{ii}}{1 - a_{ii}}\right) \\ &= \frac{1}{1 - a_{ii}}. \end{aligned}$$

## 6.3 EXTENSIONS TO HIDDEN MARKOV MODELS

So far we have considered Markov models in which each state corresponded to a deterministically observable event. Thus, the output of such sources in any given state is not random. This model is too restrictive to be applicable to many problems of interest. In this section we extend the concept of Markov models to include the case in which the observation is a probabilistic function of the state—that is, the resulting model (which is

Amazon / Zentian Limited
Exhibit 1013
Page 176